https://doi.org/10.5194/egusphere-2026-414
Preprint. Discussion started: 6 February 2026

Holocene hydro-climatic variability and multi-frequency analyses at Lake Sidi Ali (Morocco)

Johannes Schmidt[1,2,3], Markus Reichert[1], Cathleen Kertscher[1], Rik Tjallingii[4], Birgit Schneider[1], Elisabeth Dietze[5], Laura Bergmann[1], Abdelfattah Benkaddour[6], Abdeslam Mikdad[7], Sylvain Pichat[8], William Fletcher[9], Steffen Mischke[10], Christoph Zielhofer[1,2]

[1]Insitute of Geography, Leipzig University, 04103 Leipzig, Germany
[2]Historical Anthropospheres working group, LeipzigLab, Leipzig University, 04107 Leipzig, Germany
[3]Institute of Geography, Technical University Dresden, 01069 Dresden, Germany
[4]Helmholtz Centre Potsdam GFZ, Section Climate Dynamics and Landscape Evolution, 14473 Potsdam, Germany
[5]Institut of Geography, Georg August University of Göttingen, 37077 Göttingen, Germany
[6]Department of Earth Studies – Cadi Ayyad University, FST Marrakech, 40000 Marrakech, Morocco
[7]Institut National des Sciences de l'Archéologie et du Patrimoine, Rabat, Morocco
[8]Laboratoire de Geologie de Lyon (LGL-TPE), 69364 Lyon, France
[9]Department of Geography, School of Environment, Education and Development, University of Manchester, M13 9PL Manchester, UK
[10]Institute of Earth Sciences, School of Engineering and Natural Sciences, University of Iceland, 102 Reykjavík, Iceland

Correspondence to: Johannes Schmidt (j.schmidt@uni-leipzig.de)

Abstract. The North African desert margin is considered one of the most sensitive areas to future climate changes. Improved knowledge about Holocene climatic variability and environmental responses on millennial to centennial scale will help to refine scenarios related to future climate changes. During the last two decades, the recovery and compilation of Holocene records from the subtropical North Atlantic and the Mediterranean realms have improved our knowledge about the millennial-scale variability of the Western Mediterranean palaeoclimate and the Saharan dust cycle. However, the understanding on periodicities as well as potential coupling and forcing mechanisms remains poor. To detect periodicities in Holocene climatic variability and geomorphological processes, we use a Holocene sediment record from Lake Sidi Ali in the semiarid to sub-humid Middle Atlas with a robust ^{210}Pb /^{137}Cs and pollen-concentrates-based ^{14}C chronology. We use a high-resolution core scanning-XRF record, in order to distinguish between lake-internal (e.g., chemical precipitation) and lake-external (e.g., detrital input) processes. Redfit and Wavelet time series analyses reveal distinct periodicities of millennial to centennial scale. By a correlation analysis of extracted, highly significant, frequency analysis spectra, three XRF-based "Redfit Proxy Groups" (RPGs) which potentially reflect different hydro-climatic forcing mechanisms were derived. Subsequently, we integrated environmental and climatic proxies from the same core (*Cedrus* pollen abundance, magnetic susceptibility, δ^{18}O and δ^{13}C values of ostracod shells, grain-size endmembers and total organic carbon) and used their wavelet domain to improve the interpretation. Finally, we identified two main periodicity regimes that affected, on the one hand, the hydrological regime and, on the other hand, the lake productivity and catchment erosion dynamics. For RPG 1 (Ca, Sr, Ca/Ti, Sr/Ti), we identified 2 ky and 1 ky periodicities, which we interpret as precipitation/evaporation related proxies in the context of North Atlantic and solar

https://doi.org/10.5194/egusphere-2026-414
Preprint. Discussion started: 6 February 2026

forcing. For RPG 2 (Fe, Ti, K, Si/Ti), we observe 3.5 ky and 1.5 ky periodicities, which we interpret as driven by lake productivity or detrital input.

1 Introduction

North-western Africa and the Western Mediterranean are known as regions highly sensitive to climate change (Alverson et al., 2003; Giorgi, 2006). The desert margin in North Africa was significantly affected by Holocene climate changes accompanied by landscape transformations (Fletcher and Zielhofer, 2013; Ruddiman, 2014). Especially, large-scale hydro-climatic forcing mechanisms in the context of outer-tropic North Atlantic originated winter rains and the spatiotemporal evolution of the African Humid Period (AHP) are under debate (Dallmeyer et al., 2020; deMenocal et al., 2000; Zielhofer et al., 2019b). The North Atlantic-driven winter-rain variations seem to be a controlling factor of the Holocene Western Mediterranean hydro-climate and respective environmental responses (Zielhofer et al., 2019b). Regarding the AHP, it is suggested that sub-tropical airmass variations, especially enhanced and northward-shifted African monsoon precipitation patterns are the major cause for more humid conditions in the Saharan realm (Braconnot et al., 2007; Shanahan et al., 2015). However, coeval enhanced Atlantic winter rains have been argued to be necessary to reproduce proxy moisture signals in Mediterranean North Africa (Cheddadi et al., 2021). Even if the monsoonal precipitation did not reach Mediterranean Northwest Africa, further hydro-climatic effects of subtropical air masses are possible. In this context, Holocene pollen records from the Moroccan Atlas Mountains indicate variations in summer drought severities that could be caused by subtropical summer temperature variations (Campbell et al., 2017).

However, for a better understanding of large-scale and external hydro-climatic forcing as well as the influences of different air masses, time-series and frequency analyses and the detection of periodicities are of particular importance in paleoenvironmental research (Azuara et al., 2020; Kern et al., 2013; Rösch and Schmidbauer, 2018). Frequency analyses break down the respective time series into individual subharmonics. This allows the identification of long-term and short-term periodicities and periodicity changes through time (Mudelsee, 2014). Additionally, frequency analyses of time-series data can help to develop a robust understanding of proxy behaviour and coupling the extracted periodicities with other archives and climate forcings (Debret et al., 2009; Mudelsee, 2019; Sabatier et al., 2020).

Robust frequency analyses already exist from the Mediterranean Northwest Africa to the southwestern High Atlas from speleothem records. There are two speleothem records from the Middle Atlas Mountains (Grotte du Piste and Chaara caves), that cover the entire Holocene (Ait Brahim et al., 2019; Wassenburg et al., 2016). These records have been interpreted in terms of winter precipitation changes with periodicities at millennial, centennial and sub-centennial scale. Further, Sha et al. (2019) presented a speleothem record from the SW High Atlas Mountains, that seems not to be influenced by Atlantic air masses but rather tropical-monsoonal air masses. Other published speleothem records only cover the last c. 1000 years (Ait Brahim et al., 2017, 2018; Wassenburg et al., 2013) and discuss centennial-scale periodicities as Atlantic air mass variabilities in the context of changes in the North Atlantic Oscillation. In this respect, lake sediments are highly complementary to speleothem records, as these archives reflect external hydroclimatic forcing mechanisms but also dust influx, catchment erosion, and lake-internal dynamics such as chemical precipitation and biomass productivity (Aufgebauer et al., 2012; Boës et al., 2011; Cohen, 2003; Conley and Schelske, 2001; Meyers, 2003; Neff et al., 2008; Zielhofer et al., 2017b). In this context, there is a lack of high-resolution lacustrine records in Mediterranean North Africa that cover the entire Holocene suitable for frequency analyses.

Regarding lacustrine records, high resolution (mm-scale) core scanning XRF (Croudace and Rothwell, 2015; Dunlea et al., 2020) data provide the opportunity for the detection of long-term (millennial) and short-term (sub-decadal to centennial) changes in lake-system behaviour (Lauterbach et al., 2011). Typically, measured elements and associated ratios can reflect a range of lake internal and external processes (Davies et al., 2015; Kylander et al., 2011). Cohen (2003) and Davies et al. (2015) present vast collections of XRF-based proxies and relate them to lake internal or external processes. However, multiple processes can influence the elemental composition such that solitary elemental proxies must be considered alongside other proxies to enhance their interpretation, including e.g., pollen, grain-size distributions, and $\delta^{18}O$ and $\delta^{13}C$ values on ostracod shells. Overall, multi-proxy approaches can help to enhance the robustness of palaeoclimatological and environmental interpretations (Martin-Puertas et al., 2012; Sanchini et al., 2020; Unkelbach et al., 2019).

In this study, we present a high-resolution, palaeolimnological and multi-element core-scanning XRF record supplemented by medium-resolution discrete proxy data from grain size endmembers, *Cedrus* pollen, $\delta^{13}C$ and $\delta^{18}O$ values of ostracod shells, magnetic susceptibility and total organic carbon from Lake Sidi Ali in the Moroccan Middle Atlas (Zielhofer et al., 2017b, a, 2019b). This study aims to (i) identify statistically robust millennial- to centennial-scale periodicities in lake-internal and lake-external proxies using complementary stationary (Redfit) and non-stationary (wavelet) frequency analyses; (ii) group XRF-derived proxies according to similarities in their frequency behaviour in order to distinguish dominant process domains controlling sediment composition; and (iii) link these frequency-based proxy groups to hydrological, catchment-erosion and redox-sensitive processes through integration with independent non-XRF proxies. Thus, we aim to assess the temporal persistence of the identified periodicities throughout the Holocene and to explore their potential links to supra-regional climatic forcing, including North Atlantic variability and solar-paced cycles.

2 Study area

Lake Sidi Ali is located in the Middle Atlas in Morocco (33° 03’ N, 05° 00’ W, 2080 m a.s.l.), a transitional location between the wetter NW and arid SE regions of Morocco (**Fig. 1a**). The lake is considered to have developed through a combination of tectonic and karstic dynamics in the Pliocene-Quaternary period (Akdim, 2015). The catchment includes mountain ridges up to c. 2350 m a.s.l. and is characterised by steep slopes with a generally sparse vegetation cover but also including notable stands of cedar (*Cedrus atlantica*) with individual trees reaching up to more than 800 years (Copes-Gerbitz et al., 2019; Zielhofer et al., 2017a). The local climate is influenced by three major air masses (the Atlantic, the Mediterranean and the Saharan) along the NW African desert margin (Knippertz et al., 2003). Nowadays, the Middle Atlas is classified between a Cs

https://doi.org/10.5194/egusphere-2026-414
Preprint. Discussion started: 6 February 2026

and BSk *Koeppen-Geiger* climate. The regional climate is characterised by summer-drought conditions and humid spring and winter seasons driven by Atlantic and Mediterranean moisture transport. The study area has a mean annual precipitation of 487 mm and a mean annual temperature of 14.5 °C, a mean January temperature with 2.0 °C and a mean July temperature with 19.7 °C (Harris et al., 2020). The vegetation assemblages in the Middle Atlas are typically distributed along an altitudinal gradient, according to changes in temperature and moisture availability (Benabid, 1982; Campbell et al., 2017). The area around Sidi Ali is mainly dominated by *Cedrus atlantica, Quercus rotundifolia, Juniperus thurifera and Crategus* sp. (Benabid, 1982; Linares et al., 2011). However, the forest vegetation is degraded due to overgrazing and logging, and *Cedrus atlantica* shows clear signs of die-back (Cheddadi et al., 2022; Rhanem, 2011). Therefore, the current vegetation cover reflects a state of human disturbance (Copes-Gerbitz et al., 2019). Currently, the lake is seprated into two sub-basins which are divided by a basalt ridge, which merge into a single, continuous lake at high lake level stands (Barker et al., 1994; Lamb et al., 1999). The main basin reached a water depth of 38 m in September 2012 (Zielhofer et al., 2017a). The closed catchment (c. 17 km²) shows no significant surface inlet or outlet in the lake (**Fig. 1b**). Several hydro-limnological measurements show a clear stratification of the water column with anaerobic conditions in the hypolimnion in summer (Dumont et al., 1973; Zielhofer et al., 2017a). The alkaline lake (pH 9.1 – 9.7) has a specific conductivity between 1.2 and 1.6 mS/cm at the lake surface and low Ca^+ contents, which indicates evaporative conditions (Lamb et al., 1999; Zielhofer et al., 2017a).

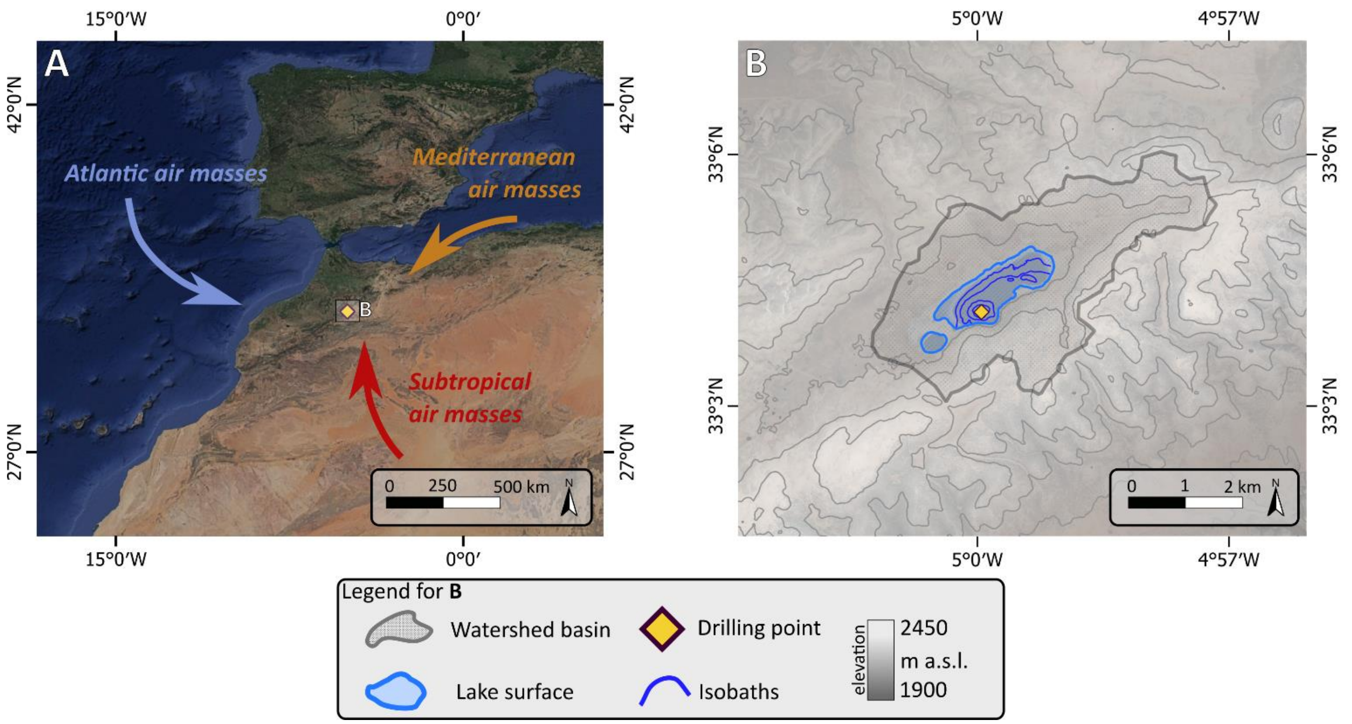

Figure 1: Geographical, climatological and topographical context of the study area. A) Location of Lake Sidi Ali in the Western Mediterranean / Northwest African context. The three major air masses influencing the Middle Atlas hydro-climate are indicated by the coloured arrows. B) Local topographical context of Lake Sidi Ali based on SRTM (NASA Shuttle Radar Topography Mission (SRTM), 2013). The contour lines have a vertical spacing of 50 m. Isobath intervals are not evenly spaced. Both panels are underlain by Google Earth satellite images (Image data: © NASA 2024, maps data: © Google 2024) (EPSG: 4326).

3 Material and methods

3.1 Data acquisition

In 2012, a 19.63 m sediment record was recovered in 2 m core sections from the deepest position of Lake Sidi Ali using a floating platform and a UWITEC piston corer. The cores show slightly laminated gyttja facies without major sedimentological shifts (Zielhofer et al., 2017a). The cores were split and the working halves were analysed by ITRAX core-scanning XRF (cs-XRF) system (Croudace and Rothwell, 2015; Zielhofer et al., 2017a) (**Tab. 1, Fig. 2a**; 1 mm intervals). The cs-XRF proxies comprise 17,863 data points for each element. Subsequently, we sampled the working half in 1-cm intervals. A total of 198 discrete samples were prepared for benchtop XRF (air-drying, 2 mm sieving, homogenisation with the planetary mill Retsch MM 200), and pressed to pellets for 2 min under 20 t of pressure (Vaneox press) (Schmidt et al., 2023b; Zielhofer et al., 2017b). The pellets were measured with a Spectro Xepos X-ray fluorescence device in a helium atmosphere (**Fig. 2a**). The Bayesian age-depth model for the Holocene sequence of lake Sidi Ali is based on AMS radiocarbon dating of 26 pollen concentrate samples accompanied by ^{210}Pb and ^{137}Cs dates for the most recent part (Fletcher et al., 2017).

The magnetic susceptibility of the cores was measured on-site using the Bartington MS2C core logging sensor, with measurements taken at 2 cm intervals (Zielhofer et al., 2017a). Samples measuring 1 cm³ in volume were prepared for pollen analysis, spaced at regular intervals of 10 cm. This method yielded a total of 201 samples (Campbell et al., 2017). Grain sizes of 124 core samples were analyzed using a Malvern Mastersizer laser diffraction particle size analyzer. Subsequently, a robust end-member modeling analysis (EMMA), employing eigenspace analysis and scaling procedures, was conducted on all non-zero grain size classes across the 124 samples using the EMMAgeo package in R (Dietze and Dietze, 2019; Zielhofer et al., 2017b). Four to six adult ostracod shells (about 20 µg) of *Fabaeformiscandona* sp. and *Candona* sp. were picked for isotope mass spectrometer analyses (δ^{13}C and δ^{18}O values) (Zielhofer et al., 2019b, a). Total organic carbon (TOC) was quantified by subtracting total inorganic carbon (TIC) determined through Scheibler carbonate measurements from total carbon (TC) values from an Elementar CNS analyzer (Zielhofer et al., 2017a).

Table 1: Data overview with temporal resolution for the Sidi Ali Holocene record parameters and references of the previous publications of the data.

Parameters	Temporal resolution	References
Cs-XRF (Ca, Fe, K, Mn, S, Si, Sr, Ti, Ca/Fe, Ca/Si, Fe/Mn, Fe/Ti, K/Ti, Mn/Ti, S/Ti, Si/Ti, Sr/Ca, Sr/Ti)	c. 1 y	Schmidt et al., 2023a; this study
Benchtop-XRF (Spectro)	c. 60 y	Schmidt et al., 2023b; Zielhofer et al., 2017b, a; this study

https://doi.org/10.5194/egusphere-2026-414
Preprint. Discussion started: 6 February 2026

Magnetic susceptibility	c. 13 y	Zielhofer et al., 2017a
Pollen (*Cedrus*)	c. 60 y	Campbell et al., 2017
Grain-size endmembers	c. 100 y	Zielhofer et al., 2017b
Ostracod shell isotopes ($\delta^{13}C$, $\delta^{18}O$)	c. 60 y	Zielhofer et al., 2019a, b
TOC	c. 40 y	Zielhofer et al., 2017a

3.2 XRF calibration

Cs-XRF elemental values given as intensities were calibrated with depth-equal benchtop-XRF results given in mg/kg using the log-ratio calibration model of the Xelerate software (Bloemsma, 2015; Weltje et al., 2015). This allows the more powerful combination of high resolution cs-XRF data with quantitative values from benchtop-XRF. For the primary selection of elements and ratios (**Fig. 2a**), we used broad compilations from Cohen (2003) and Davies et al. (2015) and previously conducted XRF element proxies from Sidi Ali core (Zielhofer et al., 2017a, b).

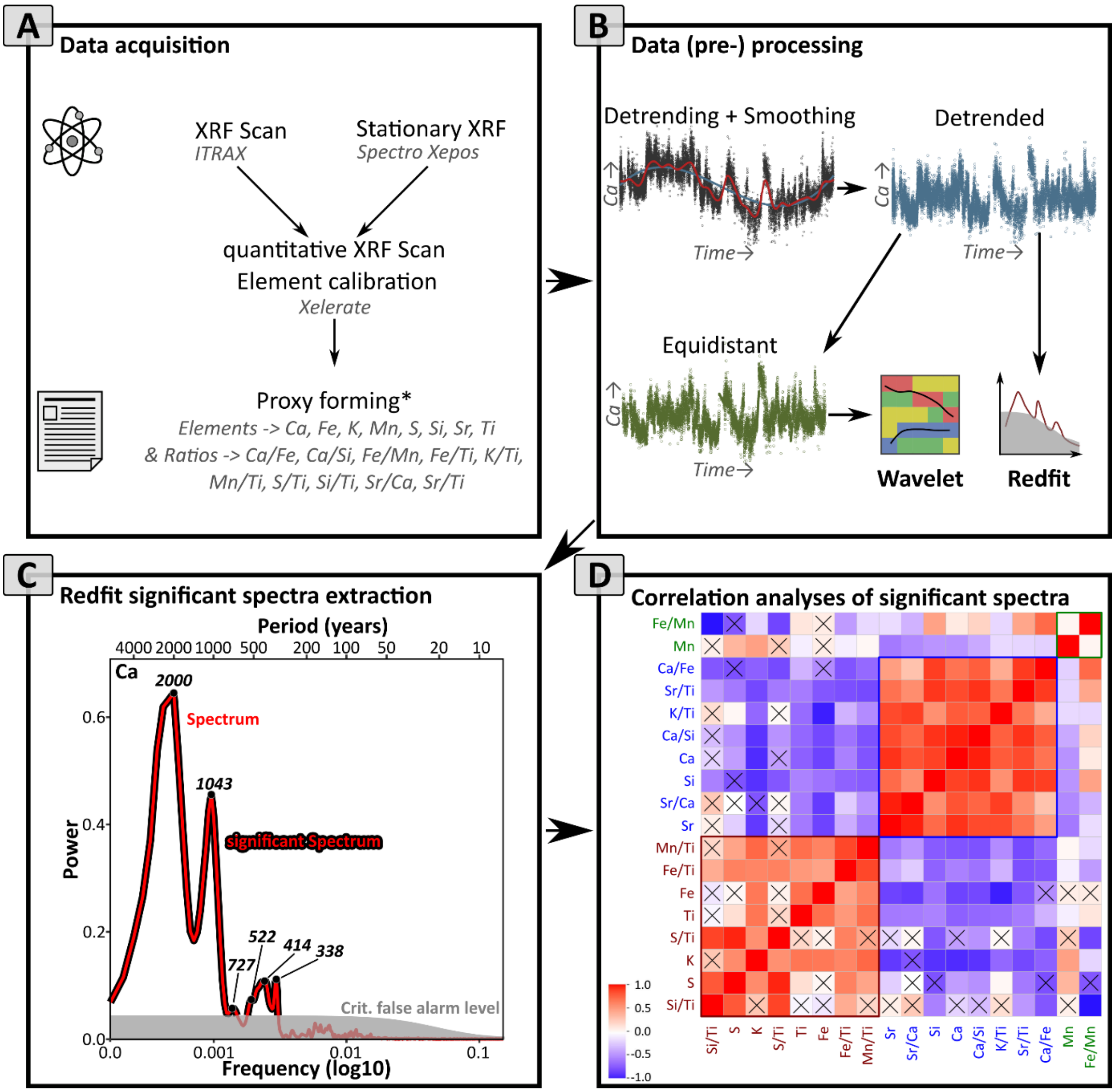

Figure 2: Flowchart of the high resolution XRF methodological approach. A) Acquisition of high resolution XRF data, calibration and forming elements and elemental ratios. *Proxy choice was done by common and published palaeolimnological XRF proxies (Cohen, 2003; Davies et al., 2015). B) Processing of high-resolution data for time series (Redfit and Wavelet) analyses, by detrending and equidistant resampling (precondition for Wavelet analyses). C) Extraction of significant (line above the critical Level of the AR1 red noise) Redfit power spectra of each proxy. D) Correlation analysis of the significant Redfit power spectra using the Spearman coefficient. The crosses show the non-significant (0.05 level) correlation values.

https://doi.org/10.5194/egusphere-2026-414
Preprint. Discussion started: 6 February 2026

3.3 Statistics

3.3.1 Data (pre-) processing

Large-scale cycle-like patterns (multi-millennial) that are not completely represented in the record can have impacts on the results from the Redfit and Wavelet analyses (Borradaile, 2003; Hochman et al., 2019; Rösch and Schmidbauer, 2018). For this reason, we detrended the data by fitting a 3rd-order polynomial regression to each proxy (**Fig. 2b**). Subsequently, we used the detrended time series for the Redfit analyses, as this method operates with unevenly spaced data (Schulz and Mudelsee, 2002). In contrast, the wavelet analysis requires equidistant spaced time series (Rösch and Schmidbauer, 2018). Debret et al. (2007) used a Spline interpolation for equidistant spacing, but we experienced "overoscillation" with artificial cyclicity for spline interpolations. Consequently, we applied a linear model on each time series using the average temporal resolution of each proxy (**Tab. 1**). The detrended and equidistant spaced time series act as input data for the wavelet analysis (**Fig. 2b**). Further, we smoothed the raw time series data by a kernel function (Härdle and Vieu, 1992) with a 500-year span, in order to extract the major positive and negative peaks in the time series for the comparison of the timing of the cycles (**Fig. 2b**, red line).

3.3.2 Redfit analysis

The Redfit algorithm works with a Lomb-Scargle Fourier transformation (Lomb, 1976; Scargle, 1982) to overcome unequal time intervals (Li et al., 2021; Schulz and Mudelsee, 2002). The process uses the Hanning window and three 50% overlapping segments (Bunn and Korpela, 2021; Schulz and Stattegger, 1997). The raw spectrum is smoothed, segmented, and linearly interpolated to eliminate artificial high frequencies and make it consistent (Ólafsdóttir et al., 2016). Finally, the averaging of all segments results in the periodogram. The significance of the periodogram was tested against the AR1 (first-order autoregressive) process, also called red noise. The red noise background is sensitive to the specific persistence of the data and therefore higher frequencies are often covered by the red noise (Mudelsee, 2014). Redfit uses Monte-Carlo simulations to create a set of AR1 processes and extracts various significance levels. We used the most conservative critical false alarm level (Schulz and Mudelsee, 2002). The dplR package (v1.7.1) (Bunn and Korpela, 2021) within the R (+ RStudio) environment (R Core Team, 2020) was used.

3.3.3 Wavelet analysis

The wavelet analysis (Torrence and Compo, 1998) also creates a periodogram, but the power of the cycles is linked with the temporal evolution. In contrast to Redfit, wavelet analysis reveals possible non-stationarities of the data (Debret et al., 2007). Periodic components get combined, and cycles and amplitudes can be displayed separately (Torrence and Compo, 1998). This procedure allows the detection of periods occurring only for a part of the time series (Debret et al., 2007). Here, the resulting

https://doi.org/10.5194/egusphere-2026-414
Preprint. Discussion started: 6 February 2026

wavelet power spectra is also tested against the AR1 process to avoid artefacts from the persistence of the data (Rösch and Schmidbauer, 2018). During the Fourier transformation, the length of the time series is increased by adding zero values to avoid false periodic events. However, this creates boundary effects as the wavelet gets closer to the edge. We avoided interpreting data within the area with increased edge effects (cone of influence) due to low accuracy of spectral information (Cazelles et al., 2008). We use the waveletComp package (v1.1) implemented by Rösch and Schmidbauer (2018) within the R environment. The algorithm uses the Morlet mother wavelet, because it keeps its shape through frequency shifts, and therefore, provides a reasonable separation from different frequency band contributors without excessive loss in temporal resolution (Cazelles et al., 2008; Goupillaud et al., 1984). The wavelet function needs equidistant spaced data (**Fig. 2b**) and we used a significance level of 95 %.

3.3.4 Correlation analysis of significant Redfit spectra

So far, cross-spectral analyses are typically bivariate, i.e. performed on pairs of proxies (Mudelsee et al., 2020; Ólafsdóttir et al., 2016). In order to reduce the dimensions (number of variables), we developed a procedure to group the proxies by using the significant spectra of the periodograms of the Redfit analyses. First, we extracted the spectrum of each XRF proxy from the Redfit periodogram. In a second step, we removed the non-significant parts of the spectra (**Fig. 2c**). The correlation analysis was done with the significant part (the values below the critical level were removed/ set to NA – "Not Available"). Due to the precondition of zero NA values throughout all variables (proxies) for a correlation analysis, we could only focus on periodicities between 1 ky and 4 ky. For power values of higher frequencies, at least one variable had NA values. However, the correlation matrix (**Fig. 2d**) shows the correlation coefficients after Spearman and the configuration of the proxies along the axes was done by similarities of positive or negative rho values.

4 Results

4.1 Dominant periodicities and inter-proxy similarities derived from Redfit analysis

The results of the Redfit analysis for 18 XRF proxies show major periodicities at c. 3.5 ky, 2ky, c. 1.5 ky, c. 1ky and several in multi-centennial scale (**Suppl. Fig. 1 - 3**). Two major groups with similar periodicity patterns are visible. As an example, the Redfit periodograms show similar periodicities for Ca and K/Ti (2 ky, c. 1 ky and some in multi-centennial scale; **Fig. 3a + b**) and S and Ti (3.5 ky, 1.5 ky and less in multi-centennial scale, **Fig. 3c + d**).

https://doi.org/10.5194/egusphere-2026-414
Preprint. Discussion started: 6 February 2026

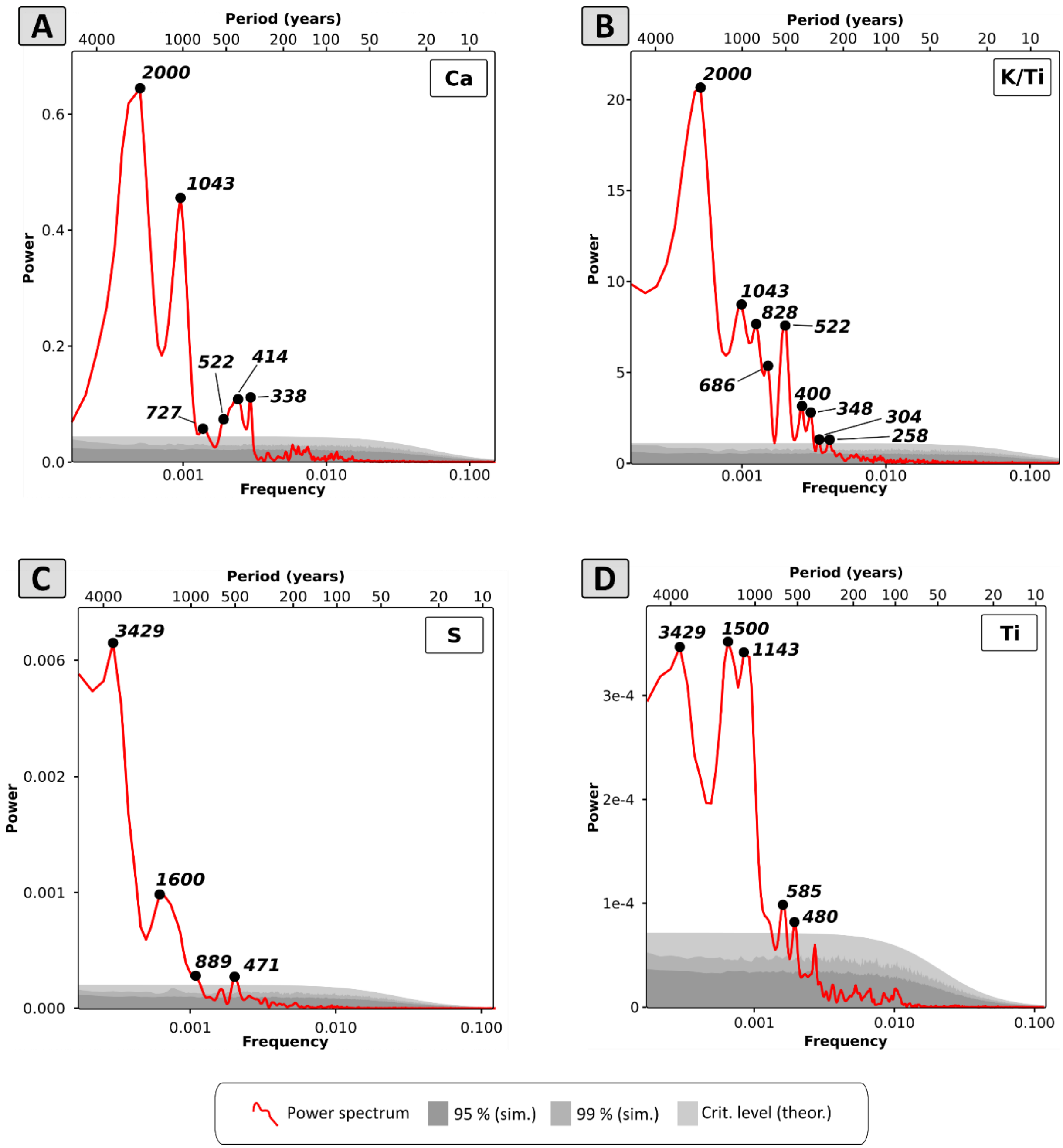

Figure 3: Redfit periodograms with significance levels of selected and calibrated cs-XRF proxies a) Ca (RPG 1), b) K/Ti ratio (RPG 1), c) S (RPG 2) and d) Ti (RPG 2). Black dots with numbers show local peaks with periodicity in years that are significant at the highest critical level. Note: X-axis is on logarithmic scale.

The correlation matrix of the significant Redfit spectra (**Fig. 2d**) shows clearly three Redfit Proxy Groups (RPG) of proxies with very similar cyclic behaviour derived from the Redfit analyses. In general, the in-group Spearman coefficients are very

https://doi.org/10.5194/egusphere-2026-414
Preprint. Discussion started: 6 February 2026

high and out-group values very low. The first RPG is dominated by Ca, Si, Sr, Ca/Fe, Ca/Si, K/Ti, Sr/Ca and Sr/Ti. The second RPG consists of Fe, K, S, Ti, Fe/Ti, Mn/Ti, S/Ti and Si/Ti. The third RPG consists of Mn and Fe/Mn.

RPG 1 has periodicities of 2 ky, 1 ky, c. 700 y and multiple modes between 600 y and 340 y (**Fig. 4**). All proxies within this group show very similar results. RPG 2 shows dominant modes of periodicity of 3.5 ky, 1.5 ky, few around 2.2 ky and between 600 y and 340 y. Fe/Ti and Mn/Ti have additional periodicities around 170 y. RPG 3 has a more diverse pattern. Mn has periodicities of 1.5 ky and 850 y and multiple modes between 600 y and 340 y. Fe/Mn has periods of c. 1.5 ky and 1 ky and several modes in the multi-centennial range. The non-XRF proxies show fewer significant periodicities. Bi- to multi-centennial cycles are present in the magnetic susceptibility, *Cedrus* pollen and $\delta^{13}C$ values. Millennial or multi-millennial periods are only present in the local endmember values, and $\delta^{13}C$ and $\delta^{18}O$ values. The TOC (total organic carbon) shows no significant cycle.

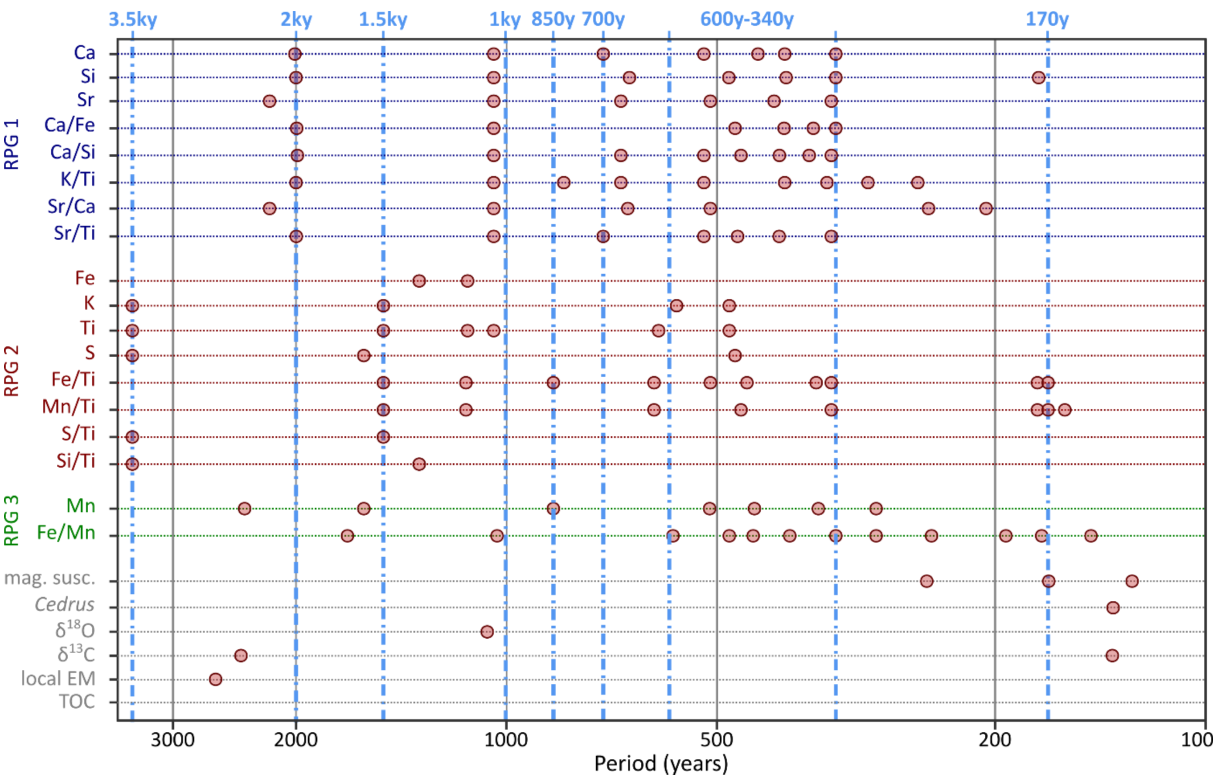

Figure 4: Synoptic graph of the positive peaks of the significant Redfit spectra of each XRF and non-XRF proxy. The x-axis is $\log_{10}$ scaled, reflects the period and the red dots show the position of the peaks. The configuration and grouping of the XRF proxies follow the results from the correlation analysis (Redfit Proxy Groups). The blue dotted lines (with labels on top of the graph) show dominant modes of periodicity of the presented proxies.

https://doi.org/10.5194/egusphere-2026-414
Preprint. Discussion started: 6 February 2026

4.2 Proxy maxima and minima during the Holocene

The first group of proxies (RPG 1, **Fig. 5**) shows dominant (absolute and secondary maxima) peaks at around 1.8 and 4.5 ka BP. The absolute and secondary minima peaks are distributed more variably through time but mostly during the Early and Middle Holocene until 6 ka BP. Within the first group the peaks of Si are distributed in opposite directions. The second group (RPG 2, **Fig. 5**) consists of two sub-groups with counter cyclical behaviour (Fe, K and Ti vs S, Fe/Ti, Mn/Ti, S/Ti and Si/Ti). Major minima and maxima of both sub-groups are located around 3.8, 4.5 and 6.6 ka BP. The third group (RPG 3, **Fig. 5**) has a more diverse peak distribution pattern with only two proxies (Mn and Fe/Mn).

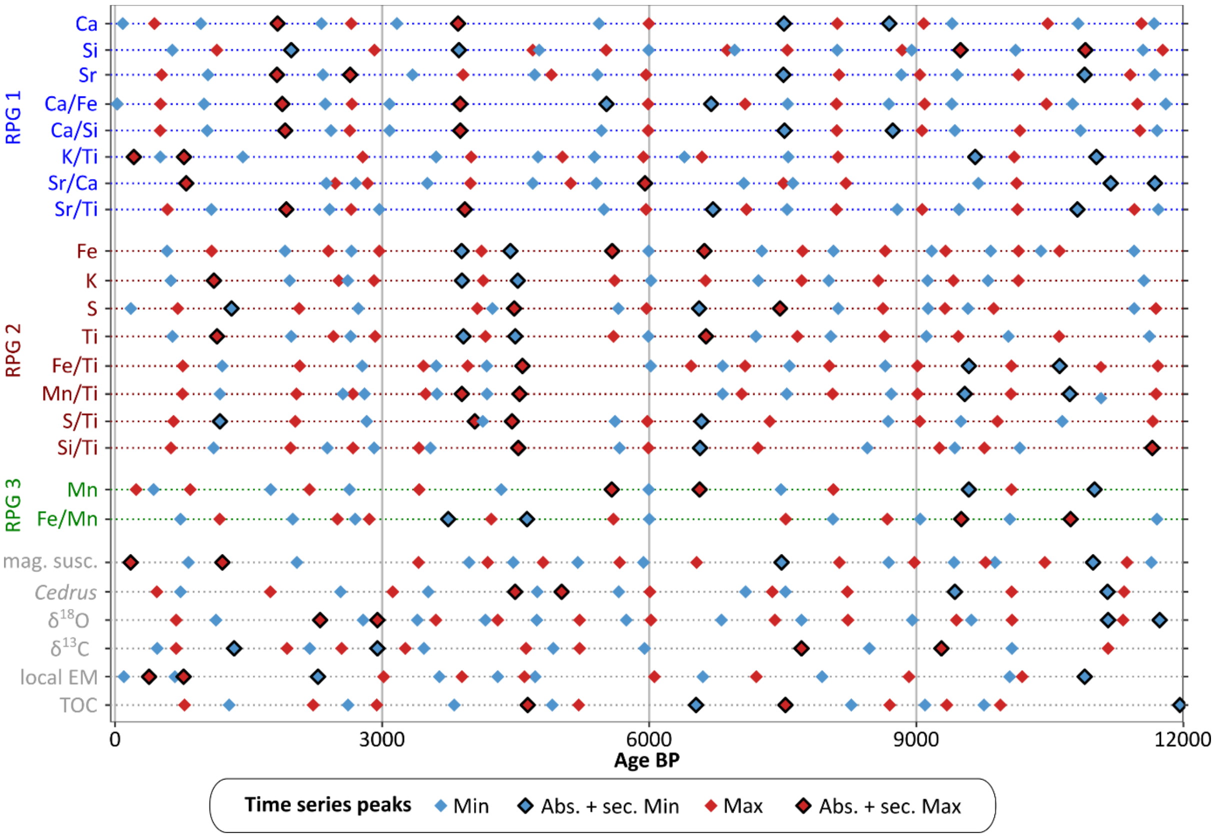

Figure 5: Minima and maxima of the smoothed time series of the selected proxies throughout the Holocene. Grey labelled proxies are non-XRF proxies. Blue diamonds reflect minima and red diamonds maxima in each time series. The encircled diamonds show the absolute and secondary minima and maxima of each time series.

4.3 Non-stationary behaviour of millennial and centennial cycles

Regarding the wavelet power spectra, Ca and K/Ti show similarities concerning millennial-scale periodicities; significant 2 ky and 1 ky cycles for the predominant parts of the Holocene (**Fig. 6a + b**). In contrast, S and Ti show periodicities of c. 3.5 ky

https://doi.org/10.5194/egusphere-2026-414
Preprint. Discussion started: 6 February 2026

and at least partly c. 1.5 ky (Ti also c. 1 ky) patterns (**Fig. 6c + d**). All wavelet power spectra of the XRF proxies can be found in the Supplementary Materials (**Suppl. Fig. 4 – 6).**

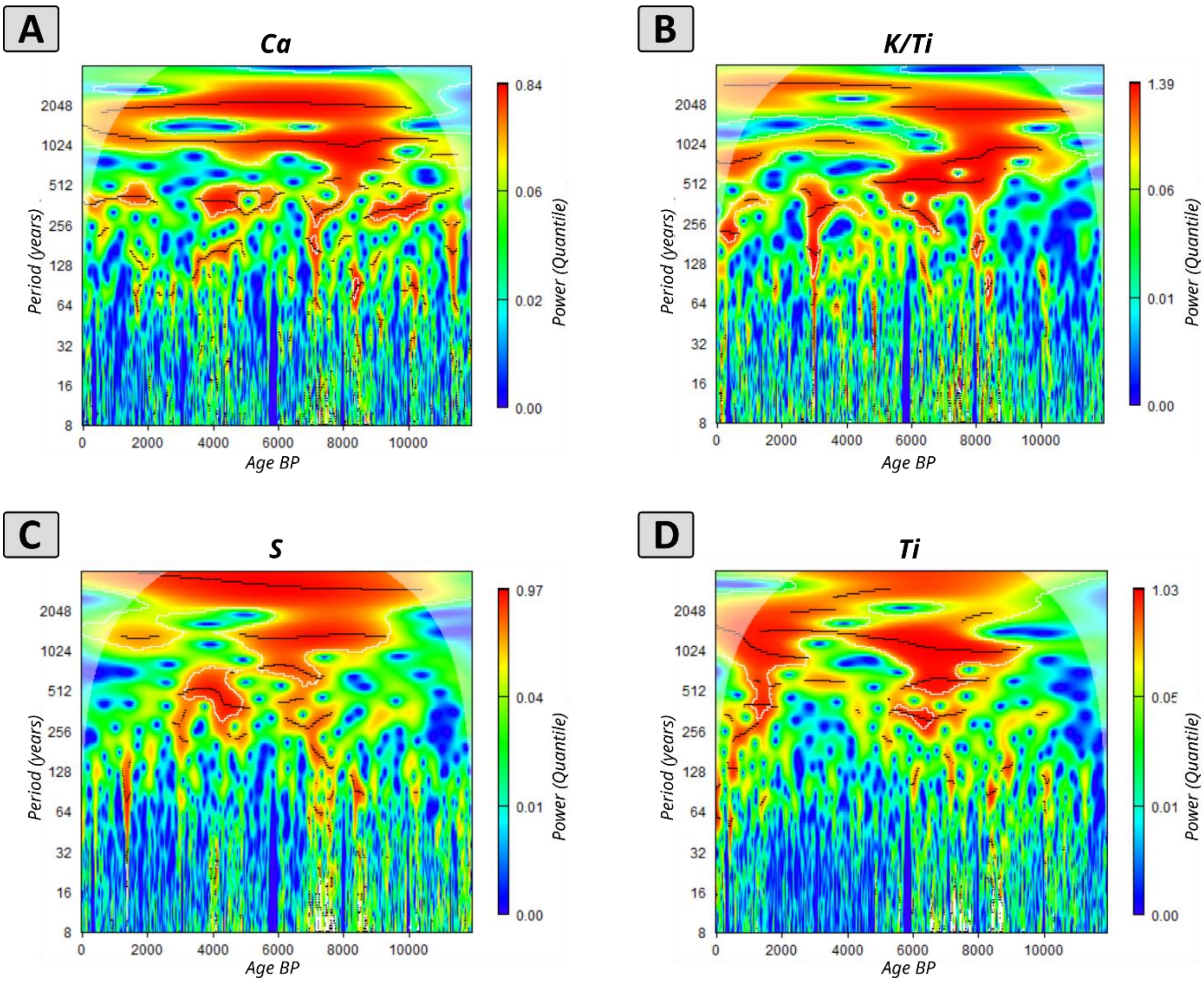

Figure 6: Exemplary wavelet power spectra of a) Ca, b) K/Ti, c) S and d) Ti. Colours show the specific power values. White lines enclose the significant areas and black lines local maxima. Grey facet shows the cone of influence.

To assess the temporal persistence of the periodicities identified by Redfit, wavelet power spectra were analysed for all proxies. There, RPG 1 show almost continuous 2 ky and 1 ky cycles throughout the Holocene (**Fig. 7**). Also, the 600 y to 340 y cycles are well represented. RPG 2 shows a clear and consistent 3.5 ky cycle pattern. In contrast to RPG 1, the 1.5 ky cycles are more dominant and much less multi-centennial cycles are apparent. RPG 3 shows a more diverse pattern but also clear multi-centennial cycles between 600 y and 340 y; mainly in the Early Holocene.

https://doi.org/10.5194/egusphere-2026-414
Preprint. Discussion started: 6 February 2026

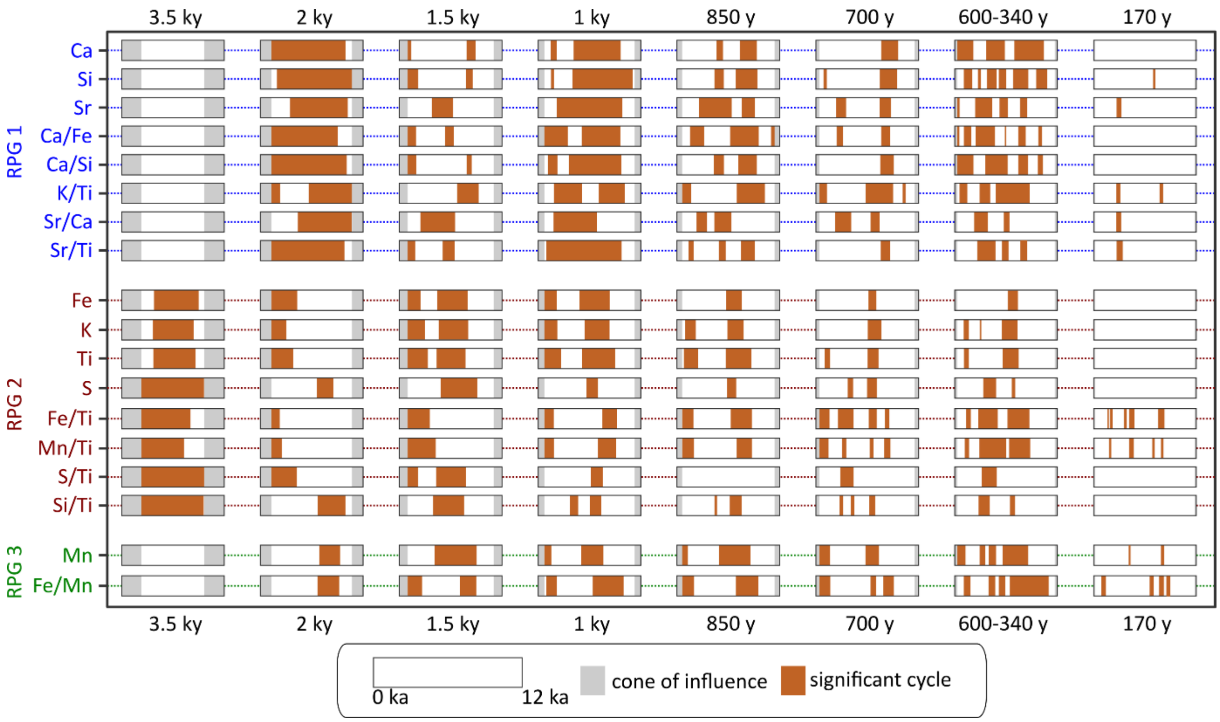

Figure 7: Synoptic graph of extracted significant wavelet power spectra of each proxy. The configuration and grouping of the proxies follow the results from the correlation analysis (Redfit Proxy Groups). The columns of the graph represent the main modes from the Redfit synoptic results (blue, dashed lines in Fig. 4). Each box reflects the whole Holocene time series. Grey bars show the cone of influence, where no significant wavelet periods were calculated due to edge effects. The red-brown colour shows the appearance of the specific cycle (see columns) throughout the Holocene, which occur within the 0.05 significance level and have a power value higher than the 80 % quantile.

5 Discussion

5.1 Numerical robustness of the frequency analyses

Hatvani et al. (2022) developed an online tool to determine the robustness of the spectral information. As the chronological uncertainty of our cs-XRF record, based on a Bayesian age-depth model, ranges from c. 500 years in the lower half up to c. 200 years in the upper parts (Fletcher et al., 2017), robust minimum periodicities that can be extracted range from c. 300 years to c. 120 years. According to that, the 170 y periodicity is less robust and has to be discussed cautiously.

5.2 Element based (XRF) proxy signals

All XRF elements reflect processes during erosion, sedimentation or post-sedimentary alterations, which might be coupled with local or regional triggers that refer to hydro-climatic changes (Bittner et al., 2020; Buggle et al., 2011; Kylander et al., 2011). However, only very rarely are all available elements from cs-XRF shown in palaeoclimate studies (Foerster et al., 2012;

https://doi.org/10.5194/egusphere-2026-414
Preprint. Discussion started: 6 February 2026

Koinig et al., 2003; Schmidt et al., 2019). Often, only selected XRF proxies are shown and used for interpretation (Cohen, 2003; Olsen et al., 2013). In general, our XRF proxies comprise conservative elements, that are geochemically fairly stable under different environmental conditions (Boës et al., 2011; Guo et al., 2019) and non-conservative elements, that are less stable and affected by biological or lake internal redox mechanisms (Bruland et al., 2014). However, the discussed XRF proxies are highly variable according to the general climatological, geomorphological and geochemical setting of their location (Davies et al., 2015; Foerster et al., 2018).

5.3 Coupling of XRF and non-XRF proxies

The integration of Sidi Ali XRF and Sidi Ali non-XRF proxies is complex in both the time domain and the frequency domain. In the time domain, some similar patterns between Sidi Ali XRF and Sidi Ali non-XRF proxies can be found; e.g. the magnetic susceptibility shows similarities with the peak distribution of Fe and Mn (**Fig. 5**). In the frequency domain, the temporal resolution of the data generally plays a crucial role in the significance of periodicities (Trauth, 2021). Checking the significance with a high-test level of the red noise of both Redfit and wavelet indicates that the results are statistically robust (Mudelsee, 2014). The number of significant periodicity peaks differs strongly between XRF and non-XRF proxies (**Fig. 4**). This is probably related to different resolutions (Yu et al., 2016). Hence, a comparison of the extracted periodicities from XRF and non-XRF proxies is also done visually and with less weight on statistical significance.

5.4 Process-based interpretation of the Redfit Proxy Groups (RPGs)

5.4.1 RPG 1 is parallel with hydroclimatic variability and corresponding changes in the precipitation/evaporation ratio

RPG 1 consists mainly of proxies related to soluble elements which are known to be sensitive to authigenic precipitation. Ca, Sr and related ratios are used in numerous studies as hydro-climatic proxy for a changing precipitation/evaporation ratio (Davies et al., 2015; Foerster et al., 2012; Kylander et al., 2011). Although Si has the same periodicity, the peaks run in exactly opposite directions (**Fig. 5**). It is a well-known phenomenon that in alkaline-rich lakes, Ca and Si abundances are opposed (Czymzik et al., 2016). Typically, this is interpreted as the dominance of internal or external processes, since Si is either formed by diatoms or is delivered as detrital input (Regattieri et al., 2016). Zielhofer et al. (2017a) argued for the Sidi Ali record, that changes in the water balance might affect the carbonate content, due to an increased relative enrichment of carbonates during low lake levels. The periodic signature of RPG 1 is dominated by 2 ky and 1 ky cycles. The latter is in accordance to the 1 ky periodicity of the hydroclimatic $\delta^{18}O$ signal from the same core (Fig. 4). Increased $\delta^{18}O$ values are in accordance with low precipitation/evaporation ratios. Specifically, multiple millennial-scale peaks in $\delta^{18}O$ during the Early and Middle Holocene (e.g., 5.0, 6.2, 8.2, 9.3 and 10.2 ka BP) reveal short-term decreases in the precipitation/evaporation ratio (Zielhofer et al., 2019b) which can be linked to RPG 1 (**Fig. 7**) and North Atlantic cooling (Bond events) (Bond et al., 2001). This reflects a

Holocene teleconnection between the North Atlantic climate and Western Mediterranean winter rain. In addition, $\delta^{13}C$ values (**Fig. 5)** are interpreted as a groundwater inflow-related proxy (Zielhofer et al., 2017a). This subterranean process is more dominant when less winter rain feeds the lake. The $\delta^{18}O$ and $\delta^{13}C$ values are anti-correlated (r = -0.62). We observe a strong c. 2 ky periodicity during the Early and Middle Holocene (until 4 ka BP) and consequently link $\delta^{13}C$ to RPG 1 (**Fig. 8f**).

The *Cedrus* pollen show for the Early to Middle Holocene a 1 ky periodicity (**Fig. 8a**). After c. 4 ka BP, the 1 ky pattern disappears and an ascending (around 1.5 ky) periodicity becomes visible. In addition, the Early Holocene 2 ky pattern prolongs until 6 ka BP. Therefore, we associate the *Cedrus* pollen abundance to RPG 1, which reveal significant 2 ky and 1 ky cycles. As discussed in Campbell et al. (2017), *Cedrus atlantica* is sensitive to prolonged summer drought. For the Early Holocene, Zielhofer et al. (2019b) discussed that *Cedrus* responded very sensitively to the orbitally-forced summer insolation maximum. Therefore, the absence of Cedar could act as summer drought proxy in the Early Holocene. Furthermore, there is a bi-millennial-scale coincidence of short-term *Cedrus* peaks at 8.2 and 10.2 ka BP and decreases in Early Holocene subtropical summer sea surface temperatures (deMenocal et al., 2000) which point to a subtropical atmospheric impact at Sidi Ali during the summer season. The TOC shows a clear c. 2 ky periodicity and some solitary 1 ky patterns (**Fig. 8c**). This fits to RPG 1. This is also supported by a high negative correlation (-0.86) between carbonates (Ca) and TOC (Zielhofer et al., 2017a). They argue that Ca and TOC are connected via aerobic/anaerobic lake-bottom conditions (organic matter preservation) due to lake-level changes.

Also belonging to RPG 1 is the K/Ti ratio, which can be used as a proxy for Saharan dust inputs. Zielhofer et al. (2017b) were able to couple the K/Ti signal from the Sidi Ali core with remote dust from the Saharan direction using provenance analyses. A peak in the K/Ti ratio at 4.2 ka BP corresponds with a hyperarid phase in the central Sahara (van der Meeren et al., 2022). The Saharan dust signal is in accordance with periodicities that are known from North Atlantic Ocean-atmosphere pattern and from monsoonal variability (Cruz et al., 2021; Gasse and Van Campo, 1994). Specifically, the Early to Middle Holocene 2 ky periodicity is known from the Saharan and Sahelian domain (Gasse and Van Campo, 1994; Tjallingii et al., 2008).

5.4.2. RPG 2 – catchment erosion and terrestrial input

This periodicity of RPG 2 is dominated by distinct 3.5 ky and 1.5 ky patterns (**Figs. 5 and 7**). However, the 3.5 ky cycles are present throughout the Holocene, whereas the 1.5 ky pattern occurs more explicitly during the Middle and the second half of the Late Holocene (**Fig. 7**). Although the 3.5 ky cycle is somewhat less trustworthy due to the short length of the total record, the dominance and grouping in the dataset seems clear.

RPG 2 consists of proxies that are known to indicate detrital influx (Fe, Ti, K, and related ratios; used and described for Sidi Ali in Zielhofer et al. (2017a) or bioproductivity (Si/Ti, S, S/Ti) processes (Davies et al., 2015; Kylander et al., 2011). Additionally, the Fe/Ti and Mn/Ti ratios show also multi-centennial (340 y – 600 y) periodicity patterns (**Figs. 5 and 7**). This corresponds partly with patterns of RPG 1 and stronger with RPG 3. The general temporal pattern of the included proxies (**Fig. 5**) shows that this group can be differentiated in two subgroups (Fe, K, Ti vs. Fe/Ti, Mn/Ti, S, S/Ti, Si/Ti). The observed

https://doi.org/10.5194/egusphere-2026-414
Preprint. Discussion started: 6 February 2026

opposing behaviour may be a result of varying detrital sedimentation rates versus a biogenetic sedimentation rate. The XRF-based interpretation is supported by the magnetic susceptibility as a local erosion proxy (Zielhofer et al., 2017a). The magnetic susceptibility shows a distinct and persistent 3.5 ky and a Middle Holocene 1.5 ky periodicity (**Fig. 8b**). Furthermore, multi-centennial periodicities are less pronounced. This pattern fits very well to RPG 2. Zielhofer et al. (2017a) reported a high correlation between Fe and magnetic susceptibility due to terrestrial input. The coarse-grained local endmember derived from grain-size EMMA is interpreted to reflect local catchment erosion and short-distance sediment supply to Lake Sidi Ali (Zielhofer et al., 2017b). However, Redfit and wavelet analyses reveal no clear or persistent expression of the ~1.5 ky and ~3.5 ky cycles in the frequency domain of this proxy (**Fig. 4 and 8d**), indicating that local erosion processes are not only paced by these millennial-scale periodicities but also by human land use and disturbance in the catchment (Bourchachen et al., 2025; Campbell et al., 2017; Cheddadi et al., 2015).

5.4.3 RPG 3 – redox-sensitivity

RPG 3 consists only of two XRF-derived proxies, Mn and Fe/Mn. Both are known as redox sensitive (Davies et al., 2015; Davison, 1993). However, Mn is more accelerated affected by redox processes compared to Fe (Boyle, 2002). Fe corresponds with RPG 2 and seems to be mainly dominated by detrital input. The effect of redox processes is strongly dominated by lake-level variations and subsequent strengths and duration of lake stratification and circulation (mictic) properties (Davies et al., 2015). The lake level of Sidi Ali is described to be controlled by winter-rain variations and its hydro-climatic consequences (Zielhofer et al., 2019b). Therefore, we assume that this group is triggered by combined processes related to RPG 1 and RPG 2. The periodicity pattern of this proxy group supports this argumentation, as it also shows patterns of both, RPG 1 and 2. The mix of c. 2 ky, 1.5 ky, 1 ky and several multi-centennial cycles is clearly in contrast to those of RPG 1 and 2 (**Figs. 5 and 7**). Fe and Mn are associated with detrital input which is also driven by catchment related processes. The subsequent redox-related alteration rather corresponds with periodicities that are associated with RPG 1. Moreover, multi-centennial periodicities occur also in redox-sensitive proxies, like the magnetic susceptibility record (**Figs. 5 and 7**).

https://doi.org/10.5194/egusphere-2026-414
Preprint. Discussion started: 6 February 2026

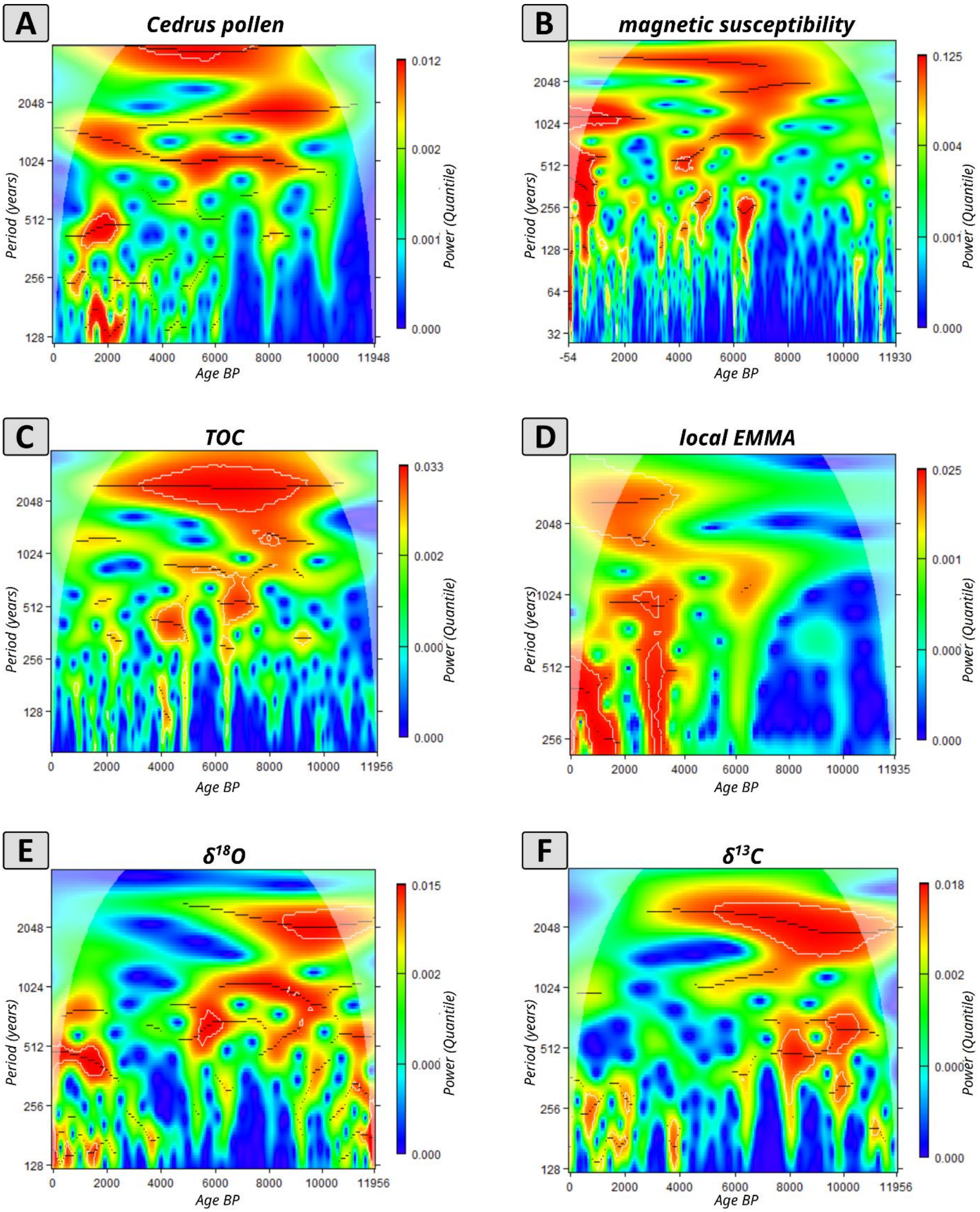

https://doi.org/10.5194/egusphere-2026-414
Preprint. Discussion started: 6 February 2026

Figure 8: Wavelet power spectra of a) *Cedrus* pollen proportion (Campbell et al., 2017), b) Magnetic susceptibility scan and c) TOC (Zielhofer et al., 2017a), d) Grain Size Endmember Analysis (EMMA) ratio (local provenance) (Zielhofer et al., 2017b), e) $\delta^{18}O$ values and f) $\delta^{13}C$ values of ostracod shells (Zielhofer et al., 2019b). Colours show the specific power values. White lines enclose the significant areas. Grey facet shows the cone of influence.

5.5 Solar cycles and their forcing on hydro-climatic variability in the Western Mediterranean

5.5.1 Hydro-climatic pattern of the bimillennial Hallstatt cycle

The bimillennial cycle is a well-known periodicity in Holocene palaeoclimate studies (Azuara et al., 2020; Goslin et al., 2018). Generally, it is considered to be triggered by solar forcing via the Hallstatt cycle (Steinhilber et al., 2012; Usoskin et al., 2016). In the North Atlantic realm, Stewart et al. (2017) presented a Bromine record from a peat bog in Scotland, which shows a distinct 2 ky cycle pattern (**Fig. 9a**). This Bromine record measured by cs-XRF reflects the storminess of the adjacent Atlantic Ocean.

Regarding the Western Mediterranean, the composite speleothem record from the Chaara Cave located in the Middle Atlas covers the entire Holocene. Ait Brahim et al. (2019) presented there a $\delta^{18}O$ value-based Western Mediterranean rainfall index. The wavelet power spectrum shows high power values for a 2 ky cycle since the Middle Holocene (**Fig. 9b**). We suggest that the Western Mediterranean precipitation/evaporation ratio might be influenced by a bi-millennial periodicity. However, the same frequency analysis for the $\delta^{18}O$ speleothem record of the nearby Grotte du Piste Cave (Wassenburg et al., 2016) did not reveal any bi-millennial periodicity (**Fig. 9c**). Hence, the climatic imprint of bi-millennial periodicities in Mediterranean hydroclimatic records remains still under debate. In contrast, a speleothem record located in the SW High Atlas Mountains (Wintimdouine Cave) is discussed as the airmass trajectory which is driven by the West African Monsoon system and consequently by the tropical realm (Sha et al., 2019). Wavelet analyses show a c. 2 ky cycle pattern (**Fig. 9d**) which is in accordance with the Saharan and sub-Saharan realm (Gasse, 2000; Gasse and Van Campo, 1994; van der Meeren et al., 2022).

https://doi.org/10.5194/egusphere-2026-414
Preprint. Discussion started: 6 February 2026

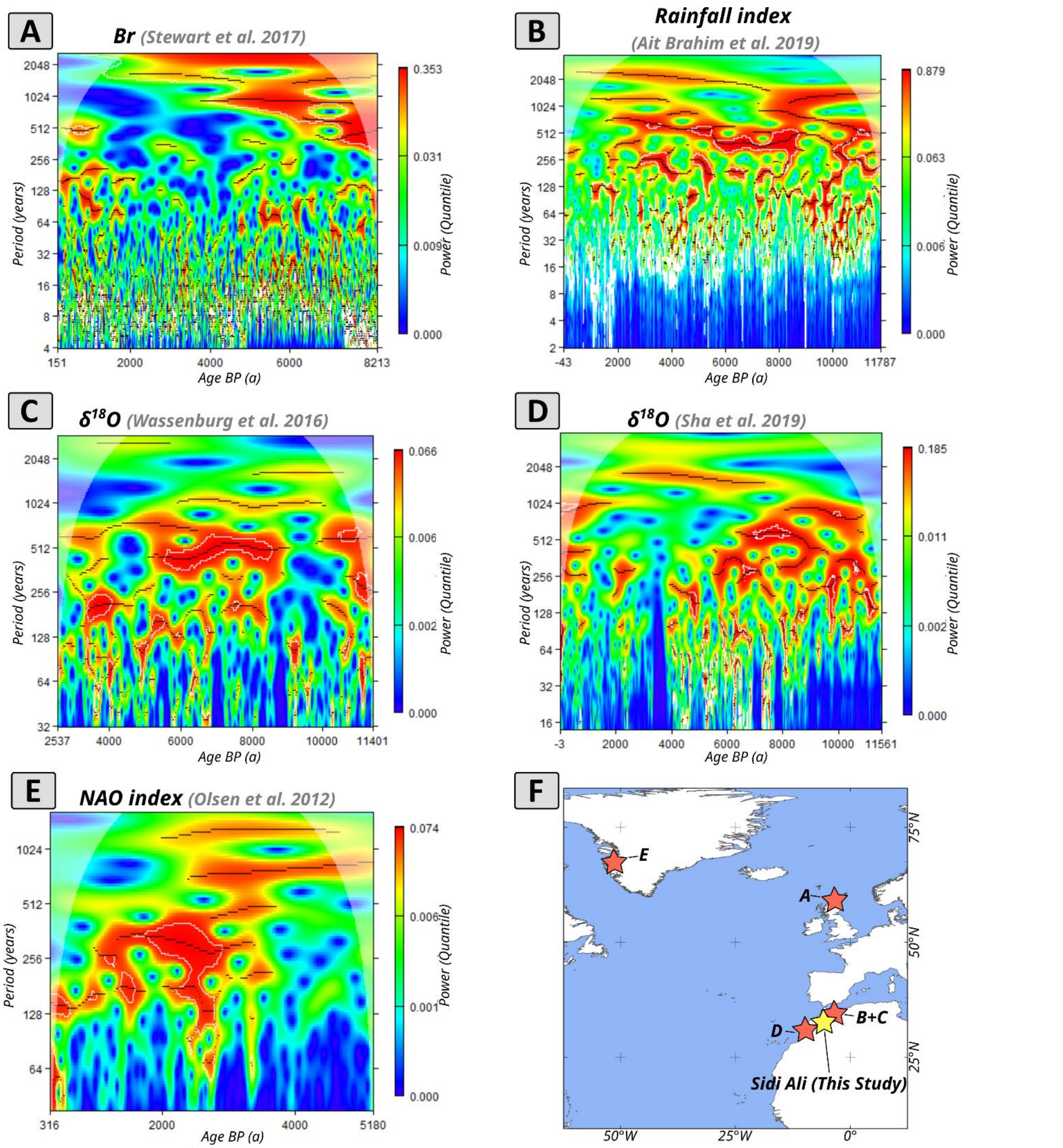

https://doi.org/10.5194/egusphere-2026-414
Preprint. Discussion started: 6 February 2026

Figure 9: Wavelet power spectra of A) Br record (Stewart et al., 2017), B) Rainfall index (Ait Brahim et al., 2019), C) $\delta^{18}O$ record from Grotte de Piste cave (Wassenburg et al., 2016) and D) $\delta^{18}O$ record from Chaara cave (Sha et al., 2019), E) NAO index (Olsen et al., 2012). Colours show the specific power values. White lines enclose the significant areas. Grey facet shows the cone of influence. Panel F shows a map of the geographic locations of the datasets presented in this figure (EPSG: 4326).

5.5.2 Hydro-climatic forcing of the millennial Eddy cycle

The eddy cycle is discussed as solar forcing mechanism behind this millennial cycle pattern (Debret et al., 2007; Steinhilber et al., 2012) and seems to affect the Atlantic precipitation regime (Zielhofer et al., 2017a). Wavelet analysis of the total solar irradiance (TSI) shows a millennial cycle which is present during the last 9.5 ka BP, although its amplitude varies through time (Steinhilber et al., 2012). The 1 ky millennial cycle is well-known in many palaeoclimatic records (Debret et al., 2009; Soon et al., 2014; Zhao et al., 2021). During the Holocene, the Scottish Shebster peat record (Stewart et al., 2017) shows a significant 1 ky cycle of North Atlantic storminess until 4 ka BP (**Fig. 9a**).
In the Western Mediterranean, the 1 ky pattern in the rainfall index from the Chaara Cave (Ait Brahim et al., 2019) seems present from the onset of the Holocene until c. 8 ka BP and again from c. 4 ka BP (**Fig. 9b**). The Grotte du Piste speleothem record (Wassenburg et al., 2016) shows only a minor, but not highly significant 1 ky cycle from c. 10 to c. 5 ka BP (**Fig. 9c**). Regarding the potential impact of sub-Saharan and Saharan air masses, the $\delta^{18}O$ record from Sha et al. (2019) does not show a clear 1 ky pattern (**Fig. 9d**). Kuhlmann et al. (2004) argues that there is a distinct border between the tropical monsoonal impact and the North Atlantic impact between 27 and 30 °N. They used the 1 ky cycle pattern for the differentiation between the two impacts. In this context, they described that there is no 1 ky periodicity in the African tropics in the Holocene.

5.5.3 Hydro-climatic forcing of multi-centennial cycles

The multi-centennial periodicity patterns cluster around 700 y and between 600 y to 340 y (**Fig. 4**). These patterns are also related to solar forcing, with unnamed cycles at c. 340 y, 500 y and 710 y (Steinhilber et al., 2012). Furthermore, Soon et al. (2014) demonstrated that the multi-centennial cycles are a result of Atlantic Ocean dynamic responses of the solar forcing. The multi-centennial periodicities are also reflected in the Moroccan speleothems from the Middle Atlas (Ait Brahim et al., 2019; Wassenburg et al., 2016; **Fig. 9b and c**), suggesting periodic winter-rain variability. The NAO record from Olsen et al. (2012) which is related to winter rain (over Greenland), also shows periodicities for the 700 y and 340 y cycles (**Fig. 9e**). Surprisingly, the Atlantic storminess record from Stewart et al. (2017) includes almost no visible multi-centennial periodicities (**Fig. 9a**). As we find the majority of multi-centennial cycles in the hydro-climatic proxy group (RPG 1), we suggest that it is dominated by Atlantic forcing mechanisms which is in accordance with Zielhofer et al. (2019b).

5.5.4 Hydro-climatic forcing of the de Vries (~200 years) cycle

The observed cycle length around 200 y is known as de Vries cycle (Steinhilber et al., 2012). The cycle has been proposed to be modulated in amplitude by the longer Hallstatt cycle, implying that its climatic imprint may vary through time rather than being continuously expressed (Komitov, 2024; Usoskin et al., 2016). Periodicities of similar lengths are found in many proxy-based studies (Ojala et al., 2015; Soon et al., 2014). Two speleothem records from North and South Morocco, that cover the last 1000 years, included c. 200 y periodicities and linked them to variations of the NAO (Ait Brahim et al., 2017, 2018). They argue that the de Vries cycle varies between dry and humid conditions. This would also affect the lake level of Sidi Ali, thus altering the redox processes at the lake floor and within the lake sediments. Accordingly, these lake-level–driven changes are reflected in the detrital proxies of RPG 2 and in the redox-sensitive proxies of RPG 3. The latter additionally exhibit a ~170 y periodicity, which may tentatively be linked to the de Vries cycle, although the statistical robustness of this specific periodicity is limited and its interpretation therefore remains cautious (see chapter 5.1).

5.5.5 Indications for a 1.5 ky cycle?

The 1.5 ky cycle in the Holocene, on the other hand, is subject of many studies (Debret et al., 2007; Fletcher et al., 2013; Soon et al., 2014). Nevertheless, there is an open debate about the frequency framing (distinct separation between 1.8 ky to 1.5 ky often not achievable, due to dating uncertainties) and the fundamental forcing of this pattern (Dima and Lohmann, 2009; Soon et al., 2014). The derived NAO index of Olsen et al. (2012) shows, even though not highly significant, a c. 1.5 ky pattern (**Fig. 9e**). Due to the time span of the NAO record, the pattern is only visible from c. 5 to c. 2 ka BP. Other studies also suggest a 1.5 ky periodicity that is stable since the Middle Holocene (Azuara et al., 2020; Smith et al., 2016). The marine record of Bond et al. (1997) shows a similar pattern, that there is a transition from 1 ky periodicity to 1.5 ky periodicity in the Middle Holocene. However, Witt and Schumann (2005) detected a significant c. 1.5 ky cycle in Greenland ice core data, which is valid for the entire Holocene. Furthermore, Soon et al. (2014) identified a persistent 1.5 ky cycle in a nitrate record in an Antarctic ice core. One can argue that the persistent Holocene-wide cycling is due to solar forcing, whereas the Middle Holocene shift from 1 ky to 1.5 ky seems to be the dynamic response of the Atlantic Ocean circulations. As we see the onset of the 1.5 ky cycle in RPG 2 in the Middle Holocene (**Fig. 7**), we assume an external forcing that is specifically affecting catchment processes and terrestrial supply. The clear mechanisms remain still unknown. The speleothem records in the Middle Atlas do not show a distinct 1.5 ky pattern (**Figs. 9b and 9c**). The speleothem record of Sha et al. (2019) from the SW High Atlas shows a c. 1.5 ky pattern between c. 7.5 and 2 ka BP, although statistically not highly significant (**Fig. 8d**). The Saharan-related processes, thus, seem to follow this pattern. Similar to the 1.5 ky pattern, the 3.5 ky periodicity is difficult to attribute to a specific forcing mechanism. It seems that catchment-related processes and local terrestrial supply differ from supra- regional North Atlantic or sub-tropical hydroclimatic forcing.

6 Conclusion

This study demonstrates that the combination of calibrated high-resolution core-scanning XRF data and multi-frequency time-series analyses (Redfit and wavelet) provides a robust framework to investigate Holocene hydro-climatic variability at the North African desert margin. The calibration approach allows quantitative interpretation of mm-scale cs-XRF data while reducing compositional effects, and the combined stationary and non-stationary spectral analyses enable both the detection and temporal evaluation of significant periodicities under conservative red-noise assumptions.

A central outcome is the identification of three Redfit Proxy Groups (RPGs) derived from correlations of significant Redfit spectra. These groups differ not only in proxy composition but also in their characteristic frequency patterns, indicating that distinct environmental processes dominated lake-system behaviour during the Holocene. RPG 1 is characterised by persistent ~2 ky and ~1 ky periodicities and additional multi-centennial modes. These proxies primarily reflect changes in the precipitation/evaporation balance, lake level and authigenic carbonate formation. Their frequency coherence with independent proxies from the same core ($\delta^{18}O$, $\delta^{13}C$, TOC and *Cedrus* pollen) indicates a dominant control by hydro-climatic variability, likely linked to North Atlantic–Western Mediterranean winter-rain dynamics. RPG 2 is dominated by ~3.5 ky and ~1.5 ky cycles and shows fewer multi-centennial periodicities. This group is interpreted to reflect catchment erosion, terrestrial input and productivity-related processes, supported by its close correspondence with the magnetic susceptibility record. The emergence of the ~1.5 ky mode mainly after the Middle Holocene suggests a temporal shift in the sensitivity of catchment processes to external forcing. RPG 3 displays mixed millennial and multi-centennial periodicities and is interpreted to record redox-sensitive lake-internal processes, integrating both hydrological and detrital influences.

Overall, the results indicate two main Holocene periodicity regimes at Lake Sidi Ali: a hydro-climatic regime dominated by ~2 ky and ~1 ky cycles, and a catchment-related regime characterised by ~3.5 ky and ~1.5 ky variability. These findings highlight that hydroclimate, productivity and erosion respond to different, only partly interacting forcing mechanisms at millennial to multi-centennial scales in Mediterranean Northwest Africa.

Data availability statement

The Spectro Xepos XRF data used for calibration are published on PANGAEA and are available under https://doi.org/10.1594/PANGAEA.960365. The cs-XRF data are published on PANGAEA and are available under https://doi.pangaea.de/10.1594/PANGAEA.960342.

Supplement link

The link to the supplement will be included by Copernicus, if applicable.

https://doi.org/10.5194/egusphere-2026-414
Preprint. Discussion started: 6 February 2026

Author contributions

JS: Conceptualization, data curation, formal analysis, investigation, methodology, visualization, validation, software, writing (original draft preparation), writing (review and editing). **MR:** data curation, formal analysis, investigation, software, writing (review and editing). **CK:** writing (review and editing). **RT:** data curation, resources, writing (review and editing). **BS:** data curation, resources, writing (review and editing). **ED:** writing (review and editing). **LB:** project administration, writing (review and editing). **AB:** funding acquisition, writing (review and editing). **AM:** writing (review and editing). **SP:** funding acquisition, writing (review and editing). **WF:** funding acquisition, writing (review and editing). **SM:** funding acquisition, writing (review and editing). **CZ:** conceptualization, funding acquisition, supervision, writing (review and editing).

Competing interests

The authors declare that they have no conflict of interest.

Disclaimer

Copernicus Publications remains neutral with regard to jurisdictional claims made in the text, published maps, institutional affiliations, or any other geographical representation in this paper. While Copernicus Publications makes every effort to include appropriate place names, the final responsibility lies with the authors. Views expressed in the text are those of the authors and do not necessarily reflect the views of the publisher.

Acknowledgements

We thank Bob McCulloch for sharing the data from the Shebster peat record. We appreciate the help of Manfred Mudelsee estimating the autocorrelation with the program TAUEST. Furthermore, we thank Michael Seidel and Sebastian Semella for their help during coding. Markus Fischer is thanked for fruitful discussions about the Holocene North African climate variability. Finally, Johannes Schmidt thanks Kalluna Kiesow for her creative "thinking outside the box" and her constant support in inspiration. We acknowledge the use of ChatGPT for language editing and stylistic polishing of the manuscript

Financial support

The authors are grateful to the German Research Foundation (DFG) for funding the related project and this study (DFG ZI 721/9-3). Additionally, the publication fee was paid by the Open Access Publishing Fund of Leipzig University, which is supported by the German Research Foundation within the program Open Access Publication Funding.

https://doi.org/10.5194/egusphere-2026-414
Preprint. Discussion started: 6 February 2026

Review statement

The review statement will be added by Copernicus Publications listing the handling editor as well as all contributing referees according to their status anonymous or identified.

References

Ait Brahim, Y., Cheng, H., Sifeddine, A., Wassenburg, J. A., Cruz, F. W., Khodri, M., Sha, L., Pérez-Zanón, N., Beraaouz, E. H., Apaéstegui, J., Guyot, J.-L., Jochum, K. P., and Bouchaou, L.: Speleothem records decadal to multidecadal hydroclimate variations in southwestern Morocco during the last millennium, Earth and Planetary Science Letters, 476, 1–10, https://doi.org/10.1016/j.epsl.2017.07.045, 2017.

Ait Brahim, Y., Wassenburg, J. A., Cruz, F. W., Sifeddine, A., Scholz, D., Bouchaou, L., Dassié, E. P., Jochum, K. P., Edwards, R. L., and Cheng, H.: Multi-decadal to centennial hydro-climate variability and linkage to solar forcing in the Western Mediterranean during the last 1000 years, Sci Rep, 8, 17446, 2018.

Ait Brahim, Y., Wassenburg, J. A., Sha, L., Cruz, F. W., Deininger, M., Sifeddine, A., Bouchaou, L., Spötl, C., Edwards, R. L., and Cheng, H.: North Atlantic Ice-Rafting, Ocean and Atmospheric Circulation During the Holocene: Insights From Western Mediterranean Speleothems, Geophys. Res. Lett., 46, 7614–7623, https://doi.org/10.1029/2019GL082405, 2019.

Akdim, B.: Karst landscape and hydrology in Morocco: research trends and perspectives, Environ Earth Sci, 74, 251–265, https://doi.org/10.1007/s12665-015-4254-5, 2015.

Alverson, K. D., Pedersen, T. F., and Bradley, R. S.: Paleoclimate, Global Change and the Future, Springer, Berlin; Heidelberg, 221 pp., https://doi.org/10.1007/978-3-642-55828-3, 2003.

Aufgebauer, A., Panagiotopoulos, K., Wagner, B., Schaebitz, F., Viehberg, F. A., Vogel, H., Zanchetta, G., Sulpizio, R., Leng, M. J., and Damaschke, M.: Climate and environmental change in the Balkans over the last 17 ka recorded in sediments from Lake Prespa (Albania/F.Y.R. of Macedonia/Greece), Quaternary International, 274, 122–135, https://doi.org/10.1016/j.quaint.2012.02.015, 2012.

Azuara, J., Sabatier, P., Lebreton, V., Jalali, B., Sicre, M.-A., Dezileau, L., Bassetti, M.-A., Frigola, J., and Combourieu-Nebout, N.: Mid- to Late-Holocene Mediterranean climate variability: Contribution of multi-proxy and multi-sequence comparison using wavelet spectral analysis in the northwestern Mediterranean basin, Earth-Science Reviews, 208, 103232, https://doi.org/10.1016/j.earscirev.2020.103232, 2020.

Barker, P. A., Roberts, N., Lamb, H. F., van der Kaars, S., and Benkaddour, A.: Interpretation of Holocene lake-level change from diatom assemblages in Lake Sidi Ali, Middle Atlas, Morocco, J Paleolimnol, 12, 223–234, https://doi.org/10.1007/BF00678022, 1994.

Benabid, A.: Bref aperçu sur la zonation altitudinale de la végétation climacique du Maroc, ecmed, 8, 301–315, https://doi.org/10.3406/ecmed.1982.1956, 1982.

Bittner, L., Bliedtner, M., Grady, D., Gil-Romera, G., Martin-Jones, C., Lemma, B., Mekonnen, B., Lamb, H. F., Yang, H., Glaser, B., Szidat, S., Salazar, G., Rose, N. L., Opgenoorth, L., Miehe, G., Zech, W., and Zech, M.: Revisiting afro-alpine Lake Garba Guracha in the Bale Mountains of Ethiopia: rationale, chronology, geochemistry, and paleoenvironmental implications, J Paleolimnol, 64, 293–314, https://doi.org/10.1007/s10933-020-00138-w, 2020.

Bloemsma, M. R.: Development of a Modelling Framework for Core Data Integration using XRF Scanning, Delft University of Technology, Delft, 229 pp., 2015.

Boës, X., Rydberg, J., Martinez-Cortizas, A., Bindler, R., and Renberg, I.: Evaluation of conservative lithogenic elements (Ti, Zr, Al, and Rb) to study anthropogenic element enrichments in lake sediments, J Paleolimnol, 46, 75–87, https://doi.org/10.1007/s10933-011-9515-z, 2011.

Bond, G., Showers, W., Cheseby, M., Lotti, R., Almasi, P., deMenocal, P. B., Priore, P., Cullen, H., Hajdas, I., and Bonani, G.: A Pervasive Millennial-Scale Cycle in North Atlantic Holocene and Glacial Climates, Science, 278, 1257–1266, https://doi.org/10.1126/science.278.5341.1257, 1997.

Bond, G., Kromer, B., Beer, J., Muscheler, R., Evans, M. N., Showers, W., Hoffmann, S., Lotti-Bond, R., Hajdas, I., and Bonani, G.: Persistent solar influence on North Atlantic climate during the Holocene, Science, 294, 2130–6, https://doi.org/10.1126/science.1065680, 2001.

Borradaile, G.: Statistics of Earth Science Data: Their Distribution in Time, Space, and Orientation, Springer Berlin Heidelberg, Berlin, Heidelberg; s.l., 351 pp., https://doi.org/10.1007/978-3-662-05223-5, 2003.

Bourchachen, M., Lemdeghri Alaoui, B., Azennoud, K., and Baali, A.: Tracing 8,000 years of climate change and human influence in the Middle Atlas, Morocco: A palynological study from Lake Iffer, Journal of African Earth Sciences, 224, 105563, https://doi.org/10.1016/j.jafrearsci.2025.105563, 2025.

Boyle, J. F.: Inorganic geochemical methods in palaeolimnology, in: Tracking Environmental Change Using Lake Sediments: Physical and Geochemical Methods, vol. 2, edited by: Last, W. M. and Smol, J. P., Kluwer Academic Publishers, Dordrecht, 83–141, 2002.

Braconnot, P., Otto-Bliesner, B., Harrison, S., Joussaume, S., Peterchmitt, J.-Y., Abe-Ouchi, A., Crucifix, M., Driesschaert, E., Fichefet, Th., Hewitt, C. D., Kageyama, M., Kitoh, A., Loutre, M.-F., Marti, O., Merkel, U., Ramstein, G., Valdes, P., Weber, L., Yu, Y., and Zhao, Y.: Results of PMIP2 coupled simulations of the Mid-Holocene and LGM - Part 2: feedbacks with emphasis on the location of the ITCZ and mid- and high latitudes heat budget, Clim. Past, 3, 279–296, 2007.

Bruland, K. W., Middag, R., and Lohan, M. C.: Controls of Trace Metals in Seawater, in: Treatise on Geochemistry, Elsevier, 19–51, 2014.

Buggle, B., Glaser, B., Hambach, U., Gerasimenko, N., and Marković, S.: An evaluation of geochemical weathering indices in loess–paleosol studies, Quaternary International, 240, 12–21, https://doi.org/10.1016/j.quaint.2010.07.019, 2011.

Bunn, A. G. and Korpela, M.: An Introduction to dplR, 2021.

Campbell, J. F. E., Fletcher, W. J., Joannin, S., Hughes, P. D., Rhanem, M., and Zielhofer, C.: Environmental Drivers of Holocene Forest Development in the Middle Atlas, Morocco, Front. Ecol. Evol., 5, 201, https://doi.org/10.3389/fevo.2017.00113, 2017.

Cazelles, B., Chavez, M., Berteaux, D., Ménard, F., Vik, J. O., Jenouvrier, S., and Stenseth, N. C.: Wavelet analysis of ecological time series, Oecologia, 156, 287–304, https://doi.org/10.1007/s00442-008-0993-2, 2008.

Cheddadi, R., Nourelbait, M., Bouaissa, O., Tabel, J., Rhoujjati, A., López-Sáez, J. A., Alba-Sánchez, F., Khater, C., Ballouche, A., Dezileau, L., and Lamb, H.: A History of Human Impact on Moroccan Mountain Landscapes, Afr Archaeol Rev, 32, 233–248, https://doi.org/10.1007/s10437-015-9186-7, 2015.

Cheddadi, R., Carré, M., Nourelbait, M., François, L., Rhoujjati, A., Manay, R., Ochoa, D., and Schefuß, E.: Early Holocene greening of the Sahara requires Mediterranean winter rainfall, Proc Natl Acad Sci U S A, 118, https://doi.org/10.1073/pnas.2024898118, 2021.

Cheddadi, R., Taberlet, P., Boyer, F., Coissac, E., Rhoujjati, A., Urbach, D., Remy, C., Khater, C., el Antry, S., Aoujdad, J., Carré, M., and Ficetola, G. F.: Priority conservation areas for Cedrus atlantica in the Atlas Mountains, Morocco, Conservation Science and Practice, 4, e12680, https://doi.org/10.1111/csp2.12680, 2022.

Cohen, A. S.: Paleolimnology: The history and evolution of lake systems, New York; Oxford University Press, Oxford, 500 pp., 2003.

Conley, D. J. and Schelske, C. L.: Biogenic Silica, in: Tracking Environmental Change Using Lake Sediments, edited by: Smol, J. P., Birks, H. J. B., Last, W. M., Bradley, R. S., and Alverson, K., Springer Netherlands, Dordrecht, 281–293, https://doi.org/10.1007/0-306-47668-1_14, 2001.

Copes-Gerbitz, K., Fletcher, W., Lageard, J. G. A., Rhanem, M., and Harrison, S. P.: Multidecadal variability in Atlas cedar growth in Northwest Africa during the last 850 years: Implications for dieback and conservation of an endangered species, Dendrochronologia (Verona), 56, 125599, https://doi.org/10.1016/j.dendro.2019.05.003, 2019.

Croudace, I. W. and Rothwell, R. G.: Micro-XRF Studies of Sediment Cores, Springer Netherlands, Dordrecht, 668 pp., https://doi.org/10.1007/978-94-017-9849-5, 2015.

Cruz, J. A., McDermott, F., Turrero, M. J., Edwards, R. L., and Martín-Chivelet, J.: Strong links between Saharan dust fluxes, monsoon strength, and North Atlantic climate during the last 5000 years, Sci Adv, 7, https://doi.org/10.1126/sciadv.abe6102, 2021.

Czymzik, M., Dreibrodt, S., Feeser, I., Adolphi, F., and Brauer, A.: Mid-Holocene humid periods reconstructed from calcite varves of the Lake Woserin sediment record (north-eastern Germany), The Holocene, 26, 935–946, https://doi.org/10.1177/0959683615622549, 2016.

Dallmeyer, A., Claussen, M., Lorenz, S. J., and Shanahan, T.: The end of the African humid period as seen by a transient comprehensive Earth system model simulation of the last 8000 years, Clim. Past, 16, 117–140, https://doi.org/10.5194/cp-16-117-2020, 2020.

Davies, S. J., Lamb, H. F., and Roberts, S. J.: Micro-XRF Core Scanning in Palaeolimnology: Recent Developments, in: Micro-XRF Studies of Sediment Cores, edited by: Croudace, I. W. and Rothwell, R. G., Springer Netherlands, Dordrecht, 189–226, 2015.

Davison, W.: Iron and manganese in lakes, Earth-Science Reviews, 34, 119–163, https://doi.org/10.1016/0012-8252(93)90029-7, 1993.

Debret, M., Bout-Roumazeilles, V., Grousset, F., Desmet, M., McManus, J. F., Massei, N., Sebag, D., Petit, J.-R., Copard, Y., and Trentesaux, A.: The origin of the 1500-year climate cycles in Holocene North-Atlantic records, Clim. Past, 3, 569–575, 2007.

Debret, M., Sebag, D., Crosta, X., Massei, N., Petit, J.-R., Chapron, E., and Bout-Roumazeilles, V.: Evidence from wavelet analysis for a mid-Holocene transition in global climate forcing, Quaternary Science Reviews, 28, 2675–2688, https://doi.org/10.1016/j.quascirev.2009.06.005, 2009.

deMenocal, P. B., Ortiz, J., Guilderson, T., Adkins, J., Sarnthein, M., Baker, L., and Yarusinsky, M.: Abrupt onset and termination of the African Humid Period: rapid climate responses to gradual insolation forcing, Quaternary Science Reviews, 19, 347–361, 2000.

Dietze, E. and Dietze, M.: Grain-size distribution unmixing using the R package EMMAgeo, E&G Quaternary Sci. J., 68, 29–46, https://doi.org/10.5194/egqsj-68-29-2019, 2019.

Dima, M. and Lohmann, G.: Conceptual model for millennial climate variability: a possible combined solar-thermohaline circulation origin for the ~1,500-year cycle, Clim Dyn, 32, 301–311, https://doi.org/10.1007/s00382-008-0471-x, 2009.

Dumont, H. J., Miron, I., Dall'Asta, U., Decraemer, W., Claus, C., and Somers, D.: Limnological Aspects of Some Moroccon Atlas Lakes, with Reference to Some Physical and Chemical Variables, the Nature and Distribution of the Phyto- and Zooplankton, Including a Note on Possibilities for the Development of an Inland Fishery, Internationale Revue ges. Hydrobiol., 58, 33–60, 1973.

Dunlea, A. G., Murray, R. W., Tada, R., Alvarez-Zarikian, C. A., Anderson, C. H., Gilli, A., Giosan, L., Gorgas, T., Hennekam, R., Irino, T., Murayama, M., Peterson, L. C., Reichart, G., Seki, A., Zheng, H., and Ziegler, M.: Intercomparison of XRF Core Scanning Results From Seven Labs and Approaches to Practical Calibration, Geochem. Geophys. Geosyst., 21, https://doi.org/10.1029/2020GC009248, 2020.

Fletcher, W. J. and Zielhofer, C.: Fragility of Western Mediterranean landscapes during Holocene Rapid Climate Changes, CATENA, 103, 16–29, https://doi.org/10.1016/j.catena.2011.05.001, 2013.

Fletcher, W. J., Debret, M., and Goñi, M. F. S.: Mid-Holocene emergence of a low-frequency millennial oscillation in western Mediterranean climate: Implications for past dynamics of the North Atlantic atmospheric westerlies, The Holocene, 23, 153–166, https://doi.org/10.1177/0959683612460783, 2013.

Fletcher, W. J., Zielhofer, C., Mischke, S., Bryant, C., Xu, X., and Fink, D.: AMS radiocarbon dating of pollen concentrates in a karstic lake system, Quaternary Geochronology, 39, 112–123, https://doi.org/10.1016/j.quageo.2017.02.006, 2017.

Foerster, V., Junginger, A., Langkamp, O., Gebru, T., Asrat, A., Umer, M., Lamb, H. F., Wennrich, V., Rethemeyer, J., Nowaczyk, N., Trauth, M. H., and Schaebitz, F.: Climatic change recorded in the sediments of the Chew Bahir basin, southern Ethiopia, during the last 45,000 years, Quaternary International, 274, 25–37, https://doi.org/10.1016/j.quaint.2012.06.028, 2012.

Foerster, V., Deocampo, D. M., Asrat, A., Günter, C., Junginger, A., Krämer, K. H., Stroncik, N. A., and Trauth, M. H.: Towards an understanding of climate proxy formation in the Chew Bahir basin, southern Ethiopian Rift, Palaeogeography, Palaeoclimatology, Palaeoecology, 501, 111–123, https://doi.org/10.1016/j.palaeo.2018.04.009, 2018.

Gasse, F.: Hydrological changes in the African tropics since the Last Glacial Maximum, Quaternary Science Reviews, 19, 189–211, 2000.

Gasse, F. and Van Campo, E.: Abrupt post-glacial climate events in West Asia and North Africa monsoon domains, Earth and Planetary Science Letters, 126, 435–456, https://doi.org/10.1016/0012-821X(94)90123-6, 1994.

Giorgi, F.: Climate change hot-spots, Geophys. Res. Lett., 33, 89, https://doi.org/10.1029/2006GL025734, 2006.

Goslin, J., Fruergaard, M., Sander, L., Gałka, M., Menviel, L., Monkenbusch, J., Thibault, N., and Clemmensen, L. B.: Holocene centennial to millennial shifts in North-Atlantic storminess and ocean dynamics, Sci Rep, 8, 12778, https://doi.org/10.1038/s41598-018-29949-8, 2018.

Goupillaud, P., Grossmann, A., and Morlet, J.: Cycle-octave and related transforms in seismic signal analysis, Geoexploration, 23, 85–102, https://doi.org/10.1016/0016-7142(84)90025-5, 1984.

Guo, P., Liu, C., Wang, P., Wang, K., Yuan, H., and Li, B.: Geochemical behavior of rare elements in Paleogene saline lake sediments of the Qaidam Basin, NE Tibetan Plateau, Carbonates Evaporites, 34, 359–372, https://doi.org/10.1007/s13146-017-0394-x, 2019.

Härdle, W. and Vieu, P.: Kernel Regression Smoothing Of Time Series, J Time Series Analysis, 13, 209–232, https://doi.org/10.1111/j.1467-9892.1992.tb00103.x, 1992.

Harris, I., Osborn, T. J., Jones, P., and Lister, D.: Version 4 of the CRU TS monthly high-resolution gridded multivariate climate dataset, Sci Data, 7, 109, https://doi.org/10.1038/s41597-020-0453-3, 2020.

Hatvani, I. G., Tanos, P., Mudelsee, M., and Kern, Z.: Robust periodic signals in proxy records with chronological uncertainty and variable temporal resolution, Quaternary Science Reviews, 276, 107294, https://doi.org/10.1016/j.quascirev.2021.107294, 2022.

Hochman, A., Saaroni, H., Abramovich, F., and Alpert, P.: Artificial Detection of Lower-Frequency Periodicity in Climatic Studies by Wavelet Analysis Demonstrated on Synthetic Time Series, 10 pp., https://doi.org/10.1175/JAMC-D-18-0331.1, 2019.

Kern, A. K., Harzhauser, M., Soliman, A., Piller, W. E., and Mandic, O.: High-resolution analysis of upper Miocene lake deposits: Evidence for the influence of Gleissberg-band solar forcing, Palaeogeography, Palaeoclimatology, Palaeoecology, 370, 167–83, https://doi.org/10.1016/j.palaeo.2012.12.005, 2013.

https://doi.org/10.5194/egusphere-2026-414
Preprint. Discussion started: 6 February 2026

Knippertz, P., Christoph, M., and Speth, P.: Long-term precipitation variability in Morocco and the link to the large-scale circulation in recent and future climates, Meteorology and Atmospheric Physics, 83, 67–88, https://doi.org/10.1007/s00703-002-0561-y, 2003.

Koinig, K. A., Shotyk, W., Lotter, A. F., Ohlendorf, C., and Sturm, M.: 9000 years of geochemical evolution of lithogenic major and trace elements in the sediment of an alpine lake – the role of climate, vegetation, and land-use history, J Paleolimnol, 30, 307–320, https://doi.org/10.1023/A:1026080712312, 2003.

Komitov, B.: About the Possible Solar Nature of the ~200 yr (de Vries/Suess) and ~2000–2500 yr (Hallstadt) Cycles and Their Influences on the Earth's Climate: The Role of Solar-Triggered Tectonic Processes in General "Sun–Climate" Relationship, Atmosphere, 15, 612, https://doi.org/10.3390/atmos15050612, 2024.

Kuhlmann, H., Meggers, H., Freudenthal, T., and Wefer, G.: The transition of the monsoonal and the N Atlantic climate system off NW Africa during the Holocene, Geophys. Res. Lett., 31, 515, https://doi.org/10.1029/2004GL021267, 2004.

Kylander, M. E., Ampel, L., Wohlfarth, B., and Veres, D.: High-resolution X-ray fluorescence core scanning analysis of Les Echets (France) sedimentary sequence: new insights from chemical proxies, J. Quaternary Sci., 26, 109–117, https://doi.org/10.1002/jqs.1438, 2011.

Lamb, H. F., Roberts, N., Leng, M., Barker, P., Benkaddour, A., and van der Kaars, S.: Lake evolution in a semi-arid montane environment: response to catchment change and hydroclimatic variation, Journal of Paleolimnology, 21, 325–343, 1999.

Lauterbach, S., Brauer, A., Andersen, N., Danielopol, D. L., Dulski, P., Hüls, M., Milecka, K., Namiotko, T., Obremska, M., and Grafenstein, U.: Environmental responses to Lateglacial climatic fluctuations recorded in the sediments of pre-Alpine Lake Mondsee (northeastern Alps), J. Quaternary Sci., 26, 253–267, https://doi.org/10.1002/jqs.1448, 2011.

Li, N., Sharifi, A., Chambers, F. M., Ge, Y., Dubois, N., Gao, G., Li, D., Liu, L., Liu, H., Wang, J., Niu, H., Meng, M., Liu, Y., Zhang, G., and Jie, D.: Linking Holocene East Asian monsoon variability to solar forcing and ENSO activity: Multi-proxy evidence from a peatland in Northeastern China, The Holocene, 31, 966–982, https://doi.org/10.1177/0959683621994662, 2021.

Linares, J. C., Taïqui, L., and Camarero, J. J.: Increasing Drought Sensitivity and Decline of Atlas Cedar (Cedrus atlantica) in the Moroccan Middle Atlas Forests, Forests, 2, 777–796, https://doi.org/10.3390/f2030777, 2011.

Lomb, N. R.: Least-squares frequency analysis of unequally spaced data, Astrophys Space Sci, 39, 447–462, https://doi.org/10.1007/BF00648343, 1976.

Martin-Puertas, C., Brauer, A., Dulski, P., and Brademann, B.: Testing climate–proxy stationarity throughout the Holocene: an example from the varved sediments of Lake Meerfelder Maar (Germany), Quaternary Science Reviews, 58, 56–65, https://doi.org/10.1016/j.quascirev.2012.10.023, 2012.

van der Meeren, T., Verschuren, D., Sylvestre, F., Nassour, Y. A., Naudts, E. L., Aguilar Ortiz, L. E., Deschamps, P., Tachikawa, K., Bard, E., Schuster, M., and Abderamane, M.: A predominantly tropical influence on late Holocene hydroclimate variation in the hyperarid central Sahara, Sci Adv, 8, 1261, https://doi.org/10.1126/sciadv.abk1261, 2022.

Meyers, P. A.: Applications of organic geochemistry to paleolimnological reconstructions: a summary of examples from the Laurentian Great Lakes, Organic Geochemistry, 34, 261–289, 2003.

Mudelsee, M.: Climate Time Series Analysis, Springer International Publishing, Cham, 477 pp., https://doi.org/10.1007/978-3-319-04450-7, 2014.

Mudelsee, M.: Trend analysis of climate time series: A review of methods, Earth-Science Reviews, 190, 310–322, https://doi.org/10.1016/j.earscirev.2018.12.005, 2019.

Mudelsee, M., Albert, J., and Sirocko, F.: Weather control in radon flux time series from Schleswig-Holstein, Germany, Int J Geomath, 11, https://doi.org/10.1007/s13137-020-00156-w, 2020.

NASA Shuttle Radar Topography Mission (SRTM): Shuttle Radar Topography Mission (SRTM) Global, https://doi.org/10.5069/G9445JDF, 2013.

Neff, J. C., Ballantyne, A. P., Farmer, G. L., Mahowald, N. M., Conroy, J. L., Landry, C. C., Overpeck, J. T., Painter, T. H., Lawrence, C. R., and Reynolds, R. L.: Increasing eolian dust deposition in the western United States linked to human activity, Nature Geosci, 1, 189–195, https://doi.org/10.1038/ngeo133, 2008.

Ojala, A. E. K., Launonen, I., Holmström, L., and Tiljander, M.: Effects of solar forcing and North Atlantic oscillation on the climate of continental Scandinavia during the Holocene, Quaternary Science Reviews, 112, 153–171, https://doi.org/10.1016/j.quascirev.2015.01.021, 2015.

Ólafsdóttir, K. B., Schulz, M., and Mudelsee, M.: REDFIT-X: Cross-spectral analysis of unevenly spaced paleoclimate time series, Computers & Geosciences, 91, 11–18, https://doi.org/10.1016/j.cageo.2016.03.001, 2016.

Olsen, J., Anderson, N. J., and Knudsen, M. F.: Variability of the North Atlantic Oscillation over the past 5,200 years, Nature Geosci, 5, 808–812, https://doi.org/10.1038/ngeo1589, 2012.

Olsen, J., Anderson, N. J., and Leng, M. J.: Limnological controls on stable isotope records of late-Holocene palaeoenvironment change in SW Greenland: a paired lake study, Quaternary Science Reviews, 66, 85–95, https://doi.org/10.1016/j.quascirev.2012.10.043, 2013.

R Core Team: R: A language and environment for statistical computing., Vienna, Austria, 2020.

Regattieri, E., Giaccio, B., Galli, P., Nomade, S., Peronace, E., Messina, P., Sposato, A., Boschi, C., and Gemelli, M.: A multi-proxy record of MIS 11–12 deglaciation and glacial MIS 12 instability from the Sulmona basin (central Italy), Quaternary Science Reviews, 132, 129–145, https://doi.org/10.1016/j.quascirev.2015.11.015, 2016.

Rhanem, M.: Aridification du climat régional et remontée de la limite inférieure du cèdre de l'Atlas (Cedrus atlantica Manetti) aux confins de la plaine de Midelt (Maroc), physio-geo, 143–165, https://doi.org/10.4000/physio-geo.1983, 2011.

Rösch, A. and Schmidbauer, H.: WaveletComp 1.1: A guided tour through the R package, 58 pp., 2018.

Ruddiman, W. F.: Earth's climate: Past and future, 3. ed., Freeman, New York, NY, 445 pp., 2014.

Sabatier, P., Nicolle, M., Piot, C., Colin, C., Debret, M., Swingedouw, D., Perrette, Y., Bellingery, M.-C., Chazeau, B., Develle, A.-L., Leblanc, M., Skonieczny, C., Copard, Y., Reyss, J.-L., Malet, E., Jouffroy-Bapicot, I., Kelner, M., Poulenard, J., Didier, J., Arnaud, F., and Vannière, B.: Past African dust inputs in the western Mediterranean area controlled by the complex

https://doi.org/10.5194/egusphere-2026-414
Preprint. Discussion started: 6 February 2026

interaction between the Intertropical Convergence Zone, the North Atlantic Oscillation, and total solar irradiance, Clim. Past, 16, 283–298, https://doi.org/10.5194/cp-16-283-2020, 2020.

Sanchini, A., Szidat, S., Tylmann, W., Vogel, H., Wacnik, A., and Grosjean, M.: A Holocene high-resolution record of aquatic productivity, seasonal anoxia and meromixis from varved sediments of Lake Łazduny, North-Eastern Poland: insight from a novel multi-proxy approach, J. Quaternary Sci, 35, 1070–1080, https://doi.org/10.1002/jqs.3242, 2020.

Scargle, J. D.: Studies in astronomical time series analysis II. Statistical apsects of spectral analysis of unevenly spaced data, The Astrophysical Journal, 835–853, 1982.

Schmidt, J., Tjallingii, R., Schneider, B., Benkaddour, A., Mikdad, A., Pichat, S., Fletcher, W. J., Mischke, S., and Zielhofer, C.: Calibrated high-resolution XRF core-scanning data of Holocene lake sediments from Lake Sidi Ali, Middle Atlas Morocco, PANGAEA, https://doi.org/10.1594/PANGAEA.960342, 2023a.

Schmidt, J., Schneider, B., Tjallingii, R., Benkaddour, A., Mikdad, A., Pichat, S., Fletcher, W. J., Mischke, S., and Zielhofer, C.: Discrete bulk Spectro Xepos XRF data of Holocene lake sediments from Lake Sidi Ali, Middle Atlas, Morocco, PANGAEA, https://doi.org/10.1594/PANGAEA.960365, 2023b.

Schmidt, M., Leipe, C., Becker, F., Goslar, T., Hoelzmann, P., Mingram, J., Müller, S., Tjallingii, R., Wagner, M., and Tarasov, P. E.: A multi-proxy palaeolimnological record of the last 16,600 years from coastal Lake Kushu in northern Japan, Palaeogeography, Palaeoclimatology, Palaeoecology, 514, 613–626, https://doi.org/10.1016/j.palaeo.2018.11.010, 2019.

Schulz, M. and Mudelsee, M.: REDFIT: estimating red-noise spectra directly from unevenly spaced paleoclimatic time series, Computers & Geosciences, 28, 421–426, https://doi.org/10.1016/S0098-3004(01)00044-9, 2002.

Schulz, M. and Stattegger, K.: Spectrum: spectral analysis of unevenly spaced paleoclimatic time series, Computers & Geosciences, 23, 929–945, https://doi.org/10.1016/S0098-3004(97)00087-3, 1997.

Sha, L., Ait Brahim, Y., Wassenburg, J. A., Yin, J., Peros, M., Cruz, F. W., Cai, Y., Li, H., Du, W., Zhang, H., Edwards, R. L., and Cheng, H.: How Far North Did the African Monsoon Fringe Expand During the African Humid Period? Insights From Southwest Moroccan Speleothems, Geophys. Res. Lett., 46, 14093–14102, https://doi.org/10.1029/2019GL084879, 2019.

Shanahan, T. M., McKay, N. P., Hughen, K. A., Overpeck, J. T., Otto-Bliesner, B., Heil, C. W., King, J., Scholz, C. A., and Peck, J.: The time-transgressive termination of the African Humid Period, Nature Geosci, 8, 140–144, https://doi.org/10.1038/ngeo2329, 2015.

Smith, A. C., Wynn, P. M., Barker, P. A., Leng, M. J., Noble, S. R., and Tych, W.: North Atlantic forcing of moisture delivery to Europe throughout the Holocene, Sci Rep, 6, 24745, https://doi.org/10.1038/srep24745, 2016.

Soon, W., Velasco Herrera, V. M., Selvaraj, K., Traversi, R., Usoskin, I., Chen, C.-T. A., Lou, J.-Y., Kao, S.-J., Carter, R. M., Pipin, V., Severi, M., and Becagli, S.: A review of Holocene solar-linked climatic variation on centennial to millennial timescales: Physical processes, interpretative frameworks and a new multiple cross-wavelet transform algorithm, Earth-Science Reviews, 134, 1–15, https://doi.org/10.1016/j.earscirev.2014.03.003, 2014.

Steinhilber, F., Abreu, J. A., Beer, J., Brunner, I., Christl, M., Fischer, H., Heikkilä, U., Kubik, P. W., Mann, M., McCracken, K. G., Miller, H., Miyahara, H., Oerter, H., and Wilhelms, F.: 9,400 years of cosmic radiation and solar activity from ice cores and tree rings, Proc Natl Acad Sci U S A, 109, 5967–71, https://doi.org/10.1073/pnas.1118965109, 2012.

Stewart, H., Bradwell, T., Bullard, J., Davies, S. J., Golledge, N., and McCulloch, R. D.: 8000 years of North Atlantic storminess reconstructed from a Scottish peat record: implications for Holocene atmospheric circulation patterns in Western Europe, J. Quaternary Sci., 32, 1075–1084, https://doi.org/10.1002/jqs.2983, 2017.

Tjallingii, R., Claussen, M., Stuut, J.-B. W., Fohlmeister, J., Jahn, A., Bickert, T., Lamy, F., and Röhl, U.: Coherent high- and low-latitude control of the northwest African hydrological balance, Nature Geosci, 1, 670–675, https://doi.org/10.1038/ngeo289, 2008.

Torrence, C. and Compo, G. P.: A Practical Guide to Wavelet Analysis, Bulletin of the American Meteorological Society, 79, 61–78, 1998.

Trauth, M. H.: MATLAB® Recipes for Earth Sciences, Springer International Publishing, Cham, 526 pp., https://doi.org/10.1007/978-3-030-38441-8, 2021.

Unkelbach, J., Kashima, K., Enters, D., Dulamsuren, Ch., Punsalpaamuu, G., and Behling, H.: Late Holocene (Meghalayan) palaeoenvironmental evolution inferred from multi-proxy-studies of lacustrine sediments from the Dayan Nuur region of Mongolia, Palaeogeography, Palaeoclimatology, Palaeoecology, 530, 1–14, https://doi.org/10.1016/j.palaeo.2019.05.021, 2019.

Usoskin, I. G., Gallet, Y., Lopes, F., Kovaltsov, G. A., and Hulot, G.: Solar activity during the Holocene: the Hallstatt cycle and its consequence for grand minima and maxim, A&A, 587, 150, https://doi.org/10.1051/0004-6361/201527295, 2016.

Wassenburg, J. A., Immenhauser, A., Richter, D. K., Niedermayr, A., Riechelmann, S., Fietzke, J., Scholz, D., Jochum, K. P., Fohlmeister, J., Schröder-Ritzrau, A., Sabaoui, A., Riechelmann, D. F. C., Schneider, L., and Esper, J.: Moroccan speleothem and tree ring records suggest a variable positive state of the North Atlantic Oscillation during the Medieval Warm Period, Earth and Planetary Science Letters, 375, 291–302, https://doi.org/10.1016/j.epsl.2013.05.048, 2013.

Wassenburg, J. A., Dietrich, S., Fietzke, J., Fohlmeister, J., Jochum, K. P., Scholz, D., Richter, D. K., Sabaoui, A., Spötl, C., Lohmann, G., Andreae, M. O., and Immenhauser, A.: Reorganization of the North Atlantic Oscillation during early Holocene deglaciation, Nature Geosci, 9, 602–605, https://doi.org/10.1038/NGEO2767, 2016.

Weltje, G. J., Bloemsma, M. R., Tjallingii, R., Heslop, D., Röhl, U., and Croudace, I. W.: Prediction of Geochemical Composition from XRF Core Scanner Data: A New Multivariate Approach Including Automatic Selection of Calibration Samples and Quantification of Uncertainties, in: Micro-XRF Studies of Sediment Cores, edited by: Croudace, I. W. and Rothwell, R. G., Springer Netherlands, Dordrecht, 507–534, 2015.

Witt, A. and Schumann, A. Y.: Holocene climate variability on millenial scales recorded in Greenland ice cores, Nonlinear Processes in Geophysics, 12, 345–352, 2005.

Yu, K., Hartmann, K., Nottebaum, V., Stauch, G., Lu, H., Zeeden, C., Yi, S., Wünnemann, B., and Lehmkuhl, F.: Discriminating sediment archives and sedimentary processes in the arid endorheic Ejina Basin, NW China using a robust geochemical approach, Journal of Asian Earth Sciences, 119, 128–144, https://doi.org/10.1016/j.jseaes.2016.01.016, 2016.

Zhao, X., Soon, W., and Velasco Herrera, V. M.: Holocene Millennial-Scale Solar Variability and the Climatic Responses on Earth, Universe, 7, 36, https://doi.org/10.3390/universe7020036, 2021.

Zielhofer, C., Fletcher, W. J., Mischke, S., Batist, M., Campbell, J. F. E., Joannin, S., Tjallingii, R., El Hamouti, N., Junginger, A., Stele, A., Bussmann, J., Schneider, B., Lauer, T., Spitzer, K., Strupler, M., Brachert, T., and Mikdad, A.: Atlantic forcing of Western Mediterranean winter rain minima during the last 12,000 years, Quaternary Science Reviews, 157, 29–51, https://doi.org/10.1016/j.quascirev.2016.11.037, 2017a.

Zielhofer, C., Suchodoletz, H., Fletcher, W. J., Schneider, B., Dietze, E., Schlegel, M., Schepanski, K., Weninger, B., Mischke, S., and Mikdad, A.: Millennial-scale fluctuations in Saharan dust supply across the decline of the African Humid Period, Quaternary Science Reviews, 171, 119–135, https://doi.org/10.1016/j.quascirev.2017.07.010, 2017b.

Zielhofer, C., Köhler, A., Mischke, S., Benkaddour, A., Mikdad, A., and Fletcher, W. J.: Holocene oxygen isotope data from Lake Sidi Ali, Middle Atlas, Morocco, https://doi.org/10.1594/PANGAEA.899460, 2019a.

Zielhofer, C., Köhler, A., Mischke, S., Benkaddour, A., Mikdad, A., and Fletcher, W. J.: Western Mediterranean hydro-climatic consequences of Holocene ice-rafted debris (Bond) events, Clim. Past, 15, 463–475, https://doi.org/10.5194/cp-15-463-2019, 2019b.